Hydrogeology Journal (2022) 30:1989–2012
https://doi.org/10.1007/s10040-022-02551-z

REPORT

# Storage capacity of a karst groundwater reservoir associated with a large dam in a humid subtropical canyon karst area in southwestern China

Cheng Zeng[1] · Chun He[1,2] · Zaihua Liu[1] · Xiaoyu Gong[1,2] · Wangguang Chen[1,2] · Yongjun Zeng[3] · Junzu Deng[4]

Received: 28 June 2021 / Accepted: 20 September 2022 / Published online: 5 October 2022


## Abstract

Pingzhai Reservoir dam was built in a deep canyon of the southern tributary of the Wu River and is the main water resource used in the Hydro-junction Project to satisfy the water requirements of Central Guizhou Province in southwestern China. The interval basin (i.e., subbasin, encompassing lower reaches between the dam and the backwater end of the main stream contributing to the dam reservoir) of Pingzhai Reservoir is characterized by thick karstified carbonate strata. Hydrological and hydrogeochemical data, including the inflow of the main stream to the interval basin, the reservoir water level, rainfall, reservoir discharge, and concentrations of major ions and stable isotopes of oxygen and hydrogen in water, were collected and analyzed. A conceptual model was constructed using the back-propagation artificial neural network approach and the water balance equation was used to calculate the total storage capacity of the karst underground reservoir associated with the Pingzhai surface reservoir. The results showed that the intensively karstified Lower Triassic Yongningzhen Formation carbonate strata resulted in the creation of a karst groundwater reservoir with a macroscopic volumetric karst rate of ~5.0%. The total storage capacity of the karst underground reservoir is $(311 \pm 108) \times 10^6$ m$^3$, and it accounts for 29% of the total capacity of the Pingzhai surface reservoir. The reliability of the total storage capacity value of the karst underground reservoir was assessed by hydrochemical and stable isotopic methods. These results will aid in the joint management of surface reservoirs and associated underground reservoirs in karst canyon areas.

**Keywords** Karst · Groundwater/surface-water relations · Deep canyon · Underground reservoir · China

## Introduction

Karst water is a key part of terrestrial water resources. Freshwater from karst aquifers is most often used for human consumption and agricultural irrigation, and for the maintenance of groundwater-dependent ecosystems (Bakalowicz 2005). According to the latest analysis of the World Karst Aquifer Map (WOKAM), approximately 15.2% of the global ice-free continental surface is covered by karstifiable carbonate rock (Chen et al. 2017a; Goldscheider et al. 2020). Nearly 9.2% of the world's population consumes karst water (Stevanovic 2019); however, due to greenhouse gas emissions and climate change (Christensen et al. 2007), it is likely that both the quantity and quality of karst water resources will decline dramatically (Wada et al. 2010). Therefore, in response to the increasing stress imposed by future climate change on karst water resources, it is necessary to construct corresponding water infrastructure based on karst hydrological simulation and prediction against the backdrop of climate change to comprehensively develop and utilize the surface-water and groundwater resources in karst areas in the future.

Large dams are one of the most important types of water infrastructure for the development and comprehensive utilization of surface-water resources in hilly and mountainous karst areas. Globally, 68.9% of all surface exposures of

✉ Cheng Zeng
zengcheng@mail.gyig.ac.cn

✉ Zaihua Liu
liuzaihua@vip.gyig.ac.cn

1 State Key Laboratory of Environmental Geochemistry, Institute of Geochemistry, Chinese Academy of Sciences, Guiyang 550081, Guizhou, China

2 University of Chinese Academy of Sciences, Beijing 100049, China

3 Guizhou Water Resources Investment (Group) Limited Company, Guiyang 550081, Guizhou, China

4 School of Water Resources & Environmental Engineering, East China University of Technology, Nanchang 330013, Jiangxi, China

carbonate rocks occur in hills and mountains (Goldscheider et al. 2020). Currently, more than 50,000 large dams (dams at least 15 m high or, if between 5 and 15 m in height with a storage capacity of more than 3 million $m^3$ of water) are operational (Scudder 2019). Some of these large dams are located in hilly and mountainous karst areas. According to the statistics provided by the Water Resources Ministry of China, in 2011, there were 756 super-large reservoirs with storage capacities of greater than 100 million $m^3$ in China, of which 357 were located in southern Chinese provinces with subtropical humid karst landforms (Ministry of Water Resources, P.R. China 2012). With the construction of these large dams, the comprehensive utilization level of surface-water resources in hilly and mountainous karst areas has been greatly improved, and the local water supply, flood control, power generation, and shipping conditions have been further improved.

Research on the reservoir capacity of large dams in hilly and mountainous karst areas cannot be carried out in isolation because of the closely linked karst underground reservoirs in such areas. Previous studies related to underground reservoirs, however, have focused mostly on traditional underground reservoirs, and karst underground reservoirs affected by dam construction in karst areas usually have failed to attract sufficient attention. Traditional underground reservoirs, which store water in voids in nonsoluble rocks or unconsolidated sediments, represent a vital water resource (Du et al. 2008; Li 2007). They are typically constructed using vertical underground dams that are oriented perpendicular to the bedding planes of alluvial rivers (Onder and Yilmaz 2005). The groundwater flow is blocked in shallower aquifers by the underground dams, and the water is stored in the upper alluvial underground reservoir (Kharazi et al. 2019). The most well-known underground reservoirs are built in arid and semiarid areas (Gomes et al. 2018). In contrast to these traditional underground reservoirs, this study focused on underground reservoirs affected by a surface-water reservoir formed by damming in a karst valley. Although the actual degree of karstification can vary greatly under different geological and climatological conditions (Goldscheider and Drew 2007), it is generally believed that exposed carbonate rocks are karstified at least to some extent (Chen et al. 2017b). Surface reservoirs located in humid subtropical hilly and mountainous karst areas usually are surrounded by carbonate rocks with a high degree of karstification. A large number of dissolution pores and cavities are developed in the carbonate rocks, thus creating the required storage space volume for a karst underground reservoir affected by a surface-water reservoir. That is, the special karst hydrogeological characteristics result in a close relationship forming between the surface-water reservoir and groundwater because of damming. As a result, most surface reservoirs in carbonate areas will form twin groundwater reservoirs during the water storage process. Regarding the construction of large dams in the karst areas in southern China, it has been noted that these twin underground reservoirs can increase the water supply to the surface reservoirs, improve the stability of the water supply, and increase storage capacity during flood control (Liu and Feng 2002). Currently, however, quantitative calculations of the storage capacity of twin underground reservoirs in China have not been conducted, which is not conducive to the scientific management and safe operation of large dams in hilly and mountainous karst areas.

The objectives of this study were (1) to evaluate the storage capacity of the twin karst underground reservoirs that are closely linked with the Pingzhai Reservoir, a super-large dam located in southwestern Guizhou Province, China, and to provide basic water resource data and a decision-making basis for water resource scheduling and comprehensive utilization in central Guizhou Province; and (2) by taking the large reservoir in the humid subtropical karst mountainous area as a representative case study, to establish a methodology for calculating the capacity of the twin karst underground reservoirs based on water balance, stable isotope, and hydrochemistry methods.

## Materials and methods

### Pingzhai Reservoir

The Pingzhai Reservoir is located in Guizhou Province, which is at the center of the contiguous karst distribution area in southwestern China (Fig. 1). The reservoir supplies water mainly to Central Guizhou, which has a high degree of water resource stress. Guizhou Province (with an area of 176,000 $km^2$) is located to the east of the Yunnan-Guizhou Plateau in southwestern China. The special geological and geomorphic conditions make the water resources in Central Guizhou relatively scarce. The Guizhou Plateau has step-shaped terrain that increases in elevation from east to west; these steps have slopes that extend to the north and south of the step pattern (Fig. 2; SinoMaps Press 2018). The province contains an exposed carbonate rock surface area of 128,000 $km^2$ (Jiang et al. 2012). The humid subtropical monsoon climate conditions in this area resulted in the creation of the strongly karstified Guizhou Plateau. Some of the most common karst landforms include mogote-shallow depression karst in the Central Guizhou Plateau, peak cluster-deep depression karst on the Southern Guizhou slopes, graben basin karst, and deep canyon karst (Yuan et al. 1994; Zhang 2006; Wang et al. 2015). Many deep karst canyons have been carved by the downward cutting of the Wu and Beipan rivers (Fig. 2); these two water resources are also a major source of hydraulic power, which is a necessary component for the development of water conservancy and hydropower projects.

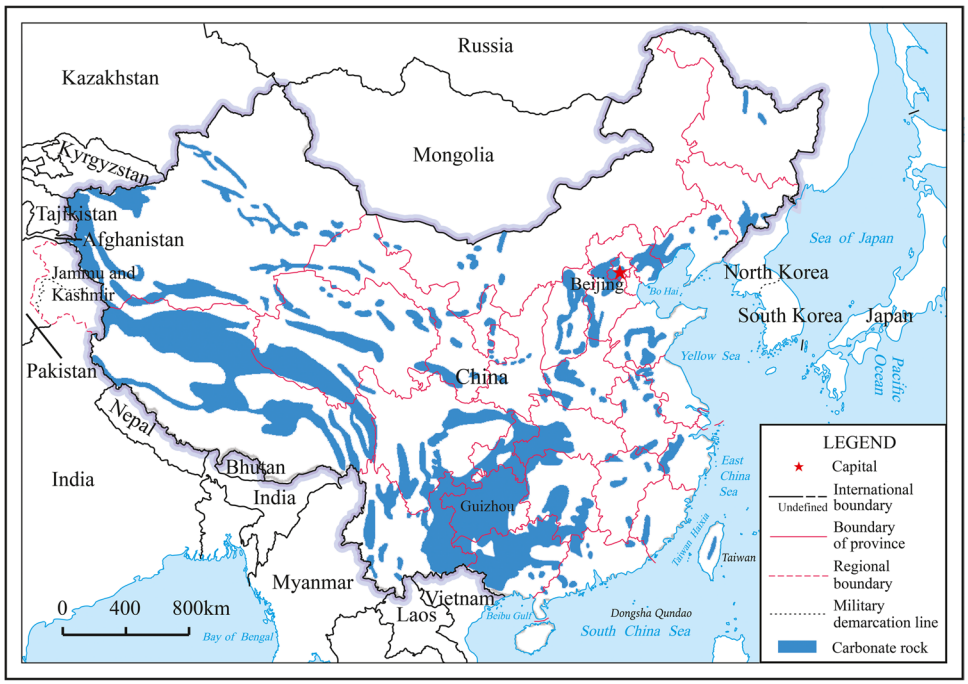


**Fig. 1** Distribution of carbonate rocks in China and the location of Guizhou Province, southwestern China

The Pingzhai Reservoir dam is located in a deep canyon of the southern tributary of Wu River (Fig. 2). Both sides of the canyon have thick karstified carbonate strata. Moreover, the hydrological data collected during the initial stage of the reservoir operation are relatively complete and readily available. As such, this reservoir was chosen as the focus of the study on the storage capacity of karst underground reservoirs.

As the main water supply for this area, the Pingzhai Reservoir is the main water resource in the Hydro-junction Project of Central Guizhou Province (Fig. 2). Two of the larger cities in the area, Guiyang and Anshun, are located on the plateau in the center of the Central Guizhou area. This economically and socially developed region is characterized by flat terrain, extensively cultivated land, and a high population density (Yang 2015). However, because the Central Guizhou Plateau is located in the wide and gentle watershed zone between the Yangtze River and the Pearl River, the resulting karstification of the carbonate strata has limited the available water supply (Meng 2013). The Hydro-junction Project was launched in November of 2009 in an effort to optimize the allocation of water resources and sustain the agricultural and urban water systems in Central Guizhou (Yuan 2015). The Hydro-junction Project is a series of projects that manage water sources, transmission, and distribution. The main water source, which stores the water and facilitates its transmission to other locations in Central Guizhou Province, is managed via a high dam in a gorge located in the middle reaches of the Sancha River (Fig. 3a, b).

This concrete-faced rockfill dam (Fig. 3a), which has a height of 162.7 m, a normal water level of 1331.0 m, a total surface-water storage capacity of $1.089 \times 10^9$ m$^3$, and an active surface-water storage capacity of $0.448 \times 10^9$ m$^3$, is located on the border between Qianzhong Village in Liuzhi County and Pingzhai Village in Zhijin County. The whole catchment area above the dam site is 3,492 km$^2$, the backwater length along the main stream of Sancha River from the Yangchang cross section to the dam site is ~38 km, and the water surface area of the reservoir is 21 km$^2$ (Fig. 4). The basin resides in an area with humid subtropical monsoon climate conditions; as such, the average annual air temperature is 15 °C, and the average annual rainfall is 1,111 mm (Meng 2013).

## Hydrogeological setting

The Guizhou Plateau consists of three major elevation steps that run from east to west. The source of the Sancha River is located in the highest step, and the Pingzhai Reservoir is located in the transition zone between the first step and the second step (Figs. 2 and 4). The area surrounding the Pingzhai Reservoir is dominated by gorges that cut deeply into the Tertiary-Quaternary mogote-depressions on the surface of Guizhou Plateau. These gorges developed due to Quaternary retrogressive erosion via the Sancha River (Fig. 3c).

The backwater end of the Pingzhai Reservoir resides in Yangchang Town in Nayong County. The interval catchment area ((i.e., subbasin, encompassing lower reaches of the surface catchment between the dam site and the backwater end of the main stream contributing to the dam reservoir) from Yangchang cross section to the Pingzhai Reservoir dam site is 815 km$^2$ (Fig. 5). The hydrogeological

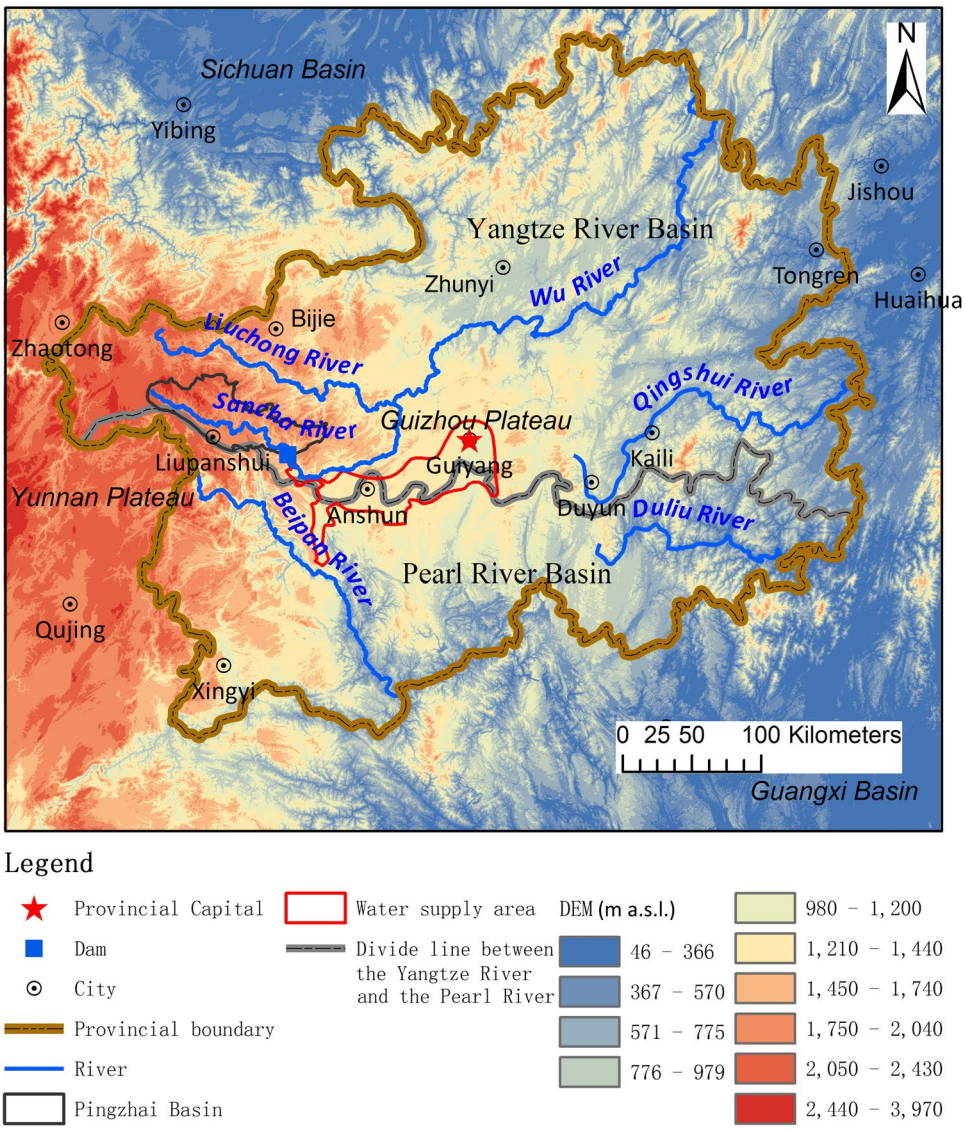


**Fig. 2** Digital elevation map (DEM, m a.s.l.) of the Hydro-junction Project in Central Guizhou Province

conditions in this area are shown in Fig. 6. The outcropping strata in the basin that lies between Yangchang Town and the dam site are paramoudras-bearing limestone from the Lower Permian Qixia Formation ($P_1q$), microcrystalline limestone from the Lower Permian Maokou Formation ($P_1m$), basalt and lithic tuff from the Upper Permian Emeishan Formation ($P_2\beta$), sandy shale and mudstone intercalated with coal seams that date to the Upper Permian ($P_2$), mudstone, sandstone, and shale intercalated with marls from the Lower Triassic Yelang Formation ($T_1y$), bedded dense limestone, dolomitic limestone, and bedded dolostone from the Lower Triassic Yongningzhen Formation ($T_1yn$), and lower mudstone and upper bedded limestone from Middle Triassic Guangling Formation ($T_2g$). The large-scale geological structure of the Pingzhai Reservoir area was formed in the middle to late stage of the Alps tectonic movement. The Baixing syncline, the Nayonghe anticline, the Shuigonghe syncline, and the Santang syncline are the main structural features in this area (Fig. 6). Due to the presence of the NW-trending Baixing syncline and the NE-trending Santang syncline, the karstified limestone and dolomitic limestone from the Lower Triassic Yongningzhen Formation form the most important synclinal water storage structure in this area (Fig. 7).

The Pingzhai Reservoir basin is thoroughly sealed. On the southwest bank of Sancha River in the Pingzhai Reservoir basin, the extension directions of the three types of impermeable strata (i.e., the $P_2\beta$, $P_2$, and $T_1y$ units) are generally oriented parallel to the southeastern flow direction of the Sancha River. These three strata are generally inclined toward the reservoir basin (Fig. 3d). Due to the impermeable shale barrier of the Lower Triassic Yelang Formation ($T_1y$), there is very little leakage into the valleys along the southern and eastern edges of the reservoir

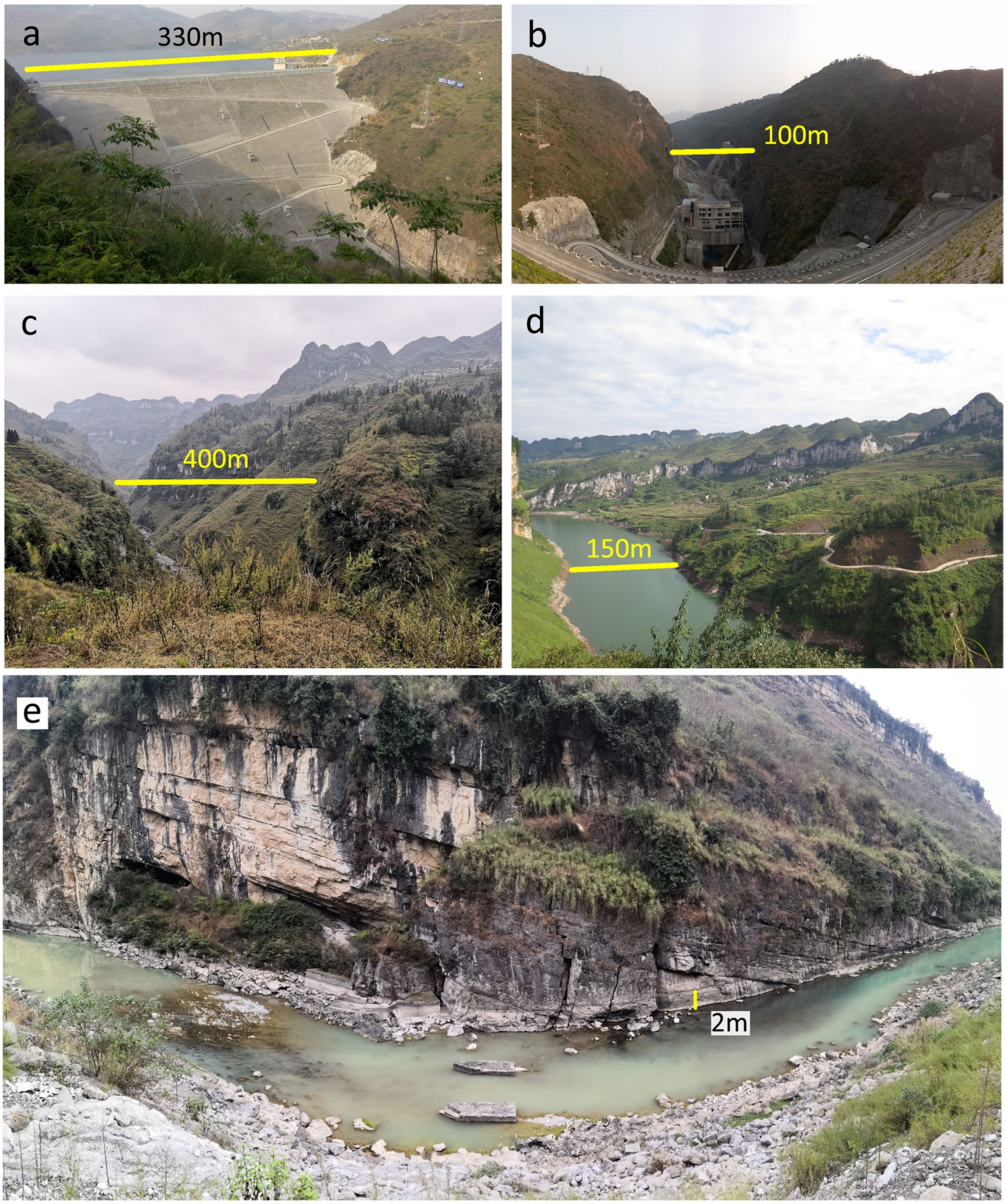


**Fig. 3** Photos from the field hydrogeological surveys. **a** Concrete faced rockfill dam at the Pingzhai Reservoir. **b** Deep canyon downstream of the dam and the power plant. **c** Shuigong gorge cutting deeply into the Tertiary-Quaternary mogote-depressions at the surface of the Guizhou Plateau. **d** Impermeable strata exposed on the southwest bank of the Sancha River. **e** Dissolved fractures and karst caves in the carbonate rocks of the Sancha River bank

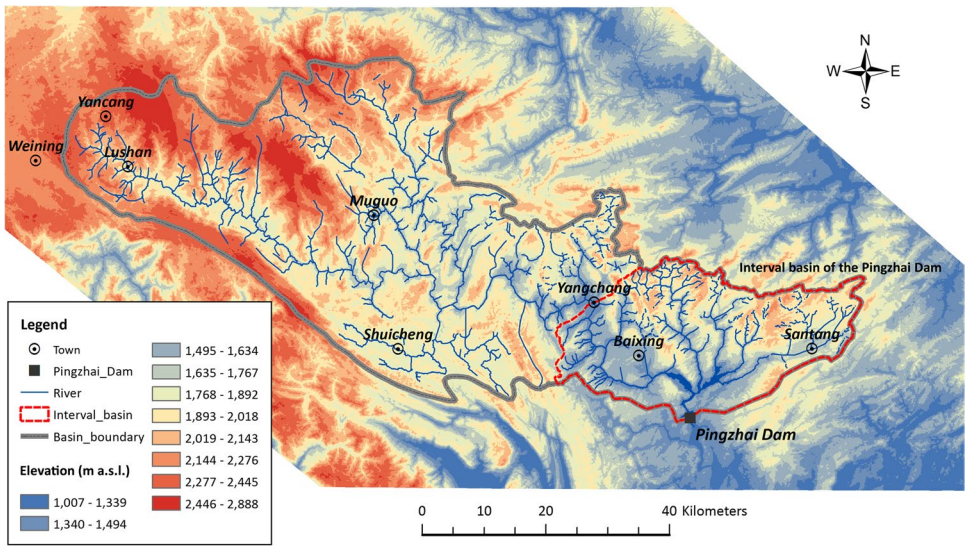


**Fig. 4** Digital elevation map (m a.s.l.) of the Sancha River Basin above the Pingzhai Reservoir dam

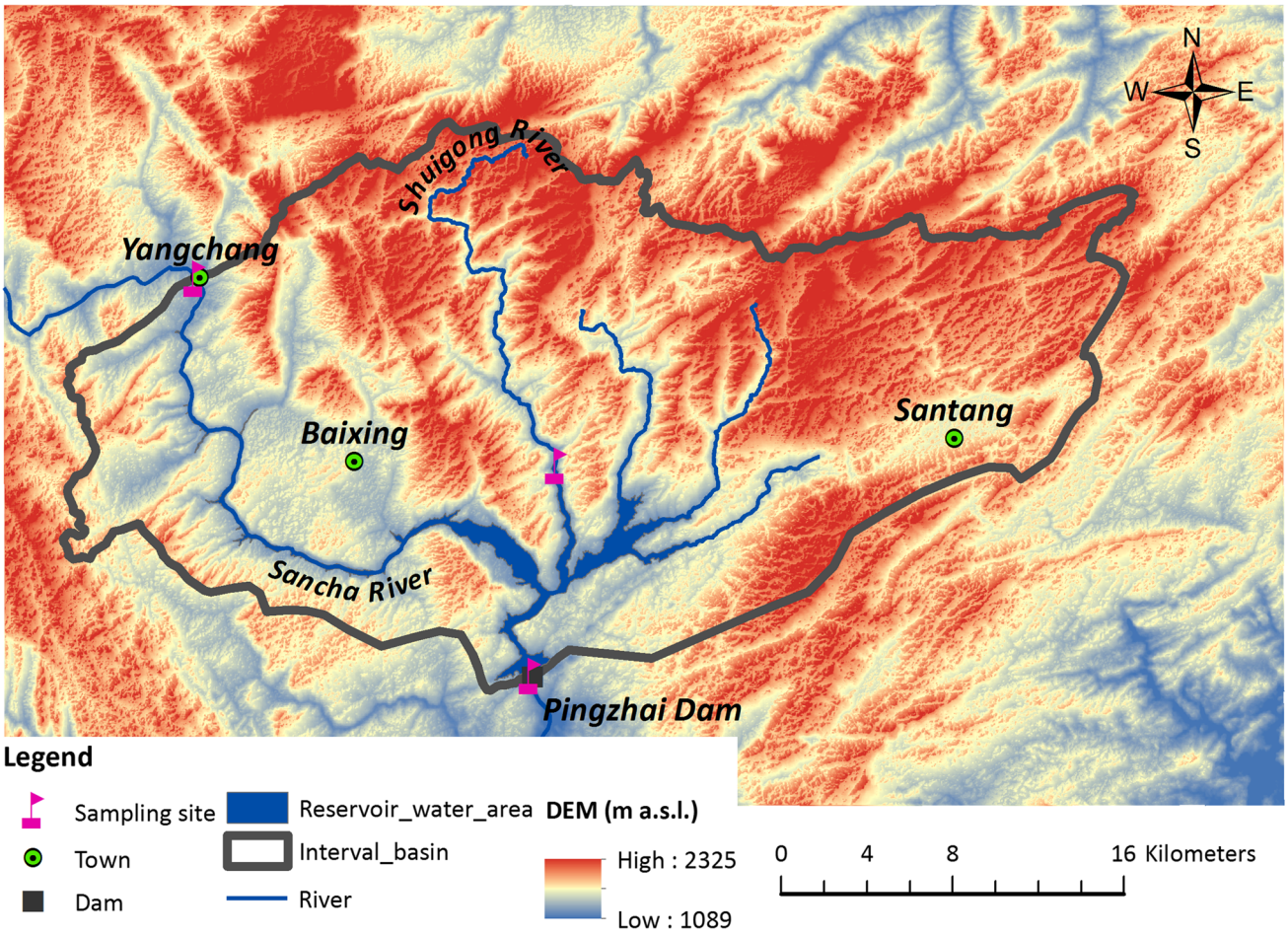


**Fig. 5** Digital elevation map (m a.s.l.) of the Pingzhai Reservoir basin between the dam and the Yangchang cross section in the main stream of the Sancha River

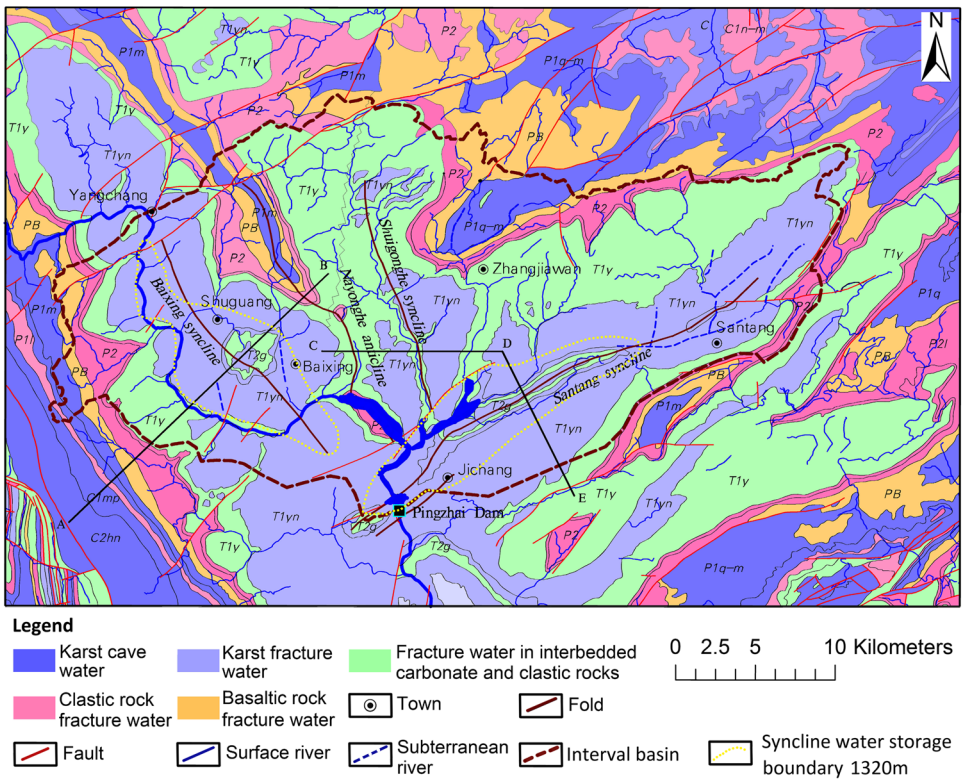


**Fig. 6** Hydrogeological map of the catchment between the Pingzhai Reservoir dam site and the backwater end of the main stream

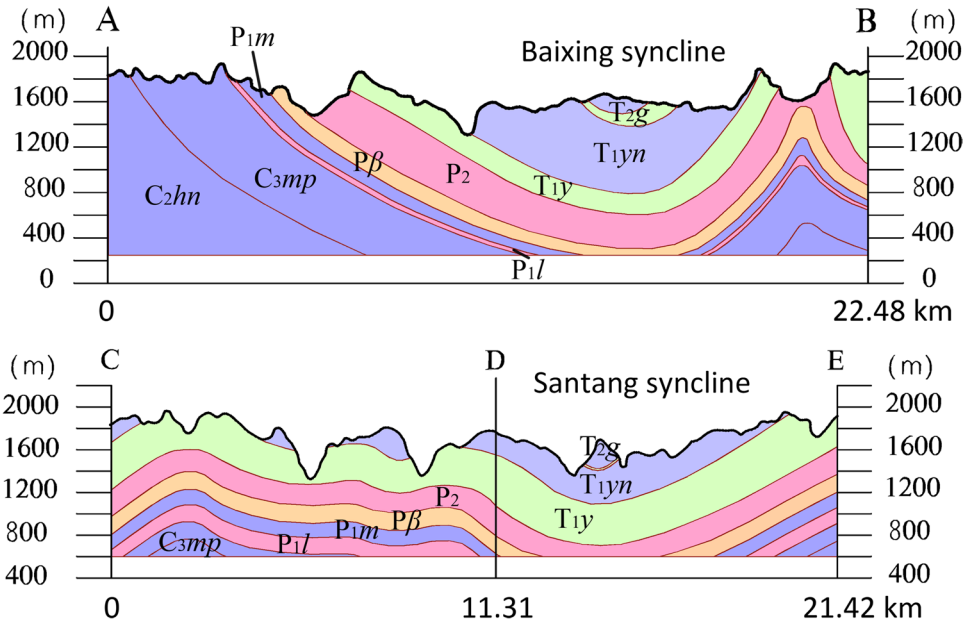


**Fig. 7** Cross sections of the Pingzhai Reservoir basin (see Fig. 6)

basin. While the karst in the limestone of the Lower Triassic Yongningzhen Formation is well developed in the head area of the Pingzhai Reservoir dam, there has been little to no seepage of water through the dam foundation or the reservoir dam abutment after the application of the curtain grouting antiseepage treatment.

## Methods to calculate the storage capacity of the associated karst groundwater reservoir

According to the hydrogeological setting of the interval basin from the Yangchang cross section to the dam site on the main stream, a water balance (budget) method was used

to calculate the storage capacity of the karst underground reservoir associated with the surface reservoir. The initial impoundment period after the completion of the Pingzhai Reservoir dam was defined as the water balance period.

This section includes two steps. First, the lateral inflow of the interval basin between the Yangchang cross section and the dam site into the reservoir-water-surface area is calculated using a monthly rainfall-runoff model based on an artificial neural network (ANN). Second, the total storage capacity of the associated karst underground reservoir is estimated using a water balance model. Figures 8 and 9 illustrate the model used here for estimating the storage capacity of the associated karst groundwater reservoir. In this section, some important formulae will be introduced.

### Water balance equations for the associated karst underground reservoir storage capacity calculation

According to the existing hydrogeological survey data of the interval basin of the Pingzhai Reservoir, the hydrogeological conditions can be summarized into four characteristics. Firstly, the gullies of the study area have down-incised violently and the drainage density is high, leading to a steep terrain. Most of the atmospheric precipitation is converted into surface runoff ($R_s$), only a small amount of atmospheric precipitation infiltrates underground and is converted into groundwater, and the depth of the water table is large (Fig. 9; Tian et al. 1979). Secondly, the slopes of the tributaries of Sancha River are large, and most of the direct runoff in the

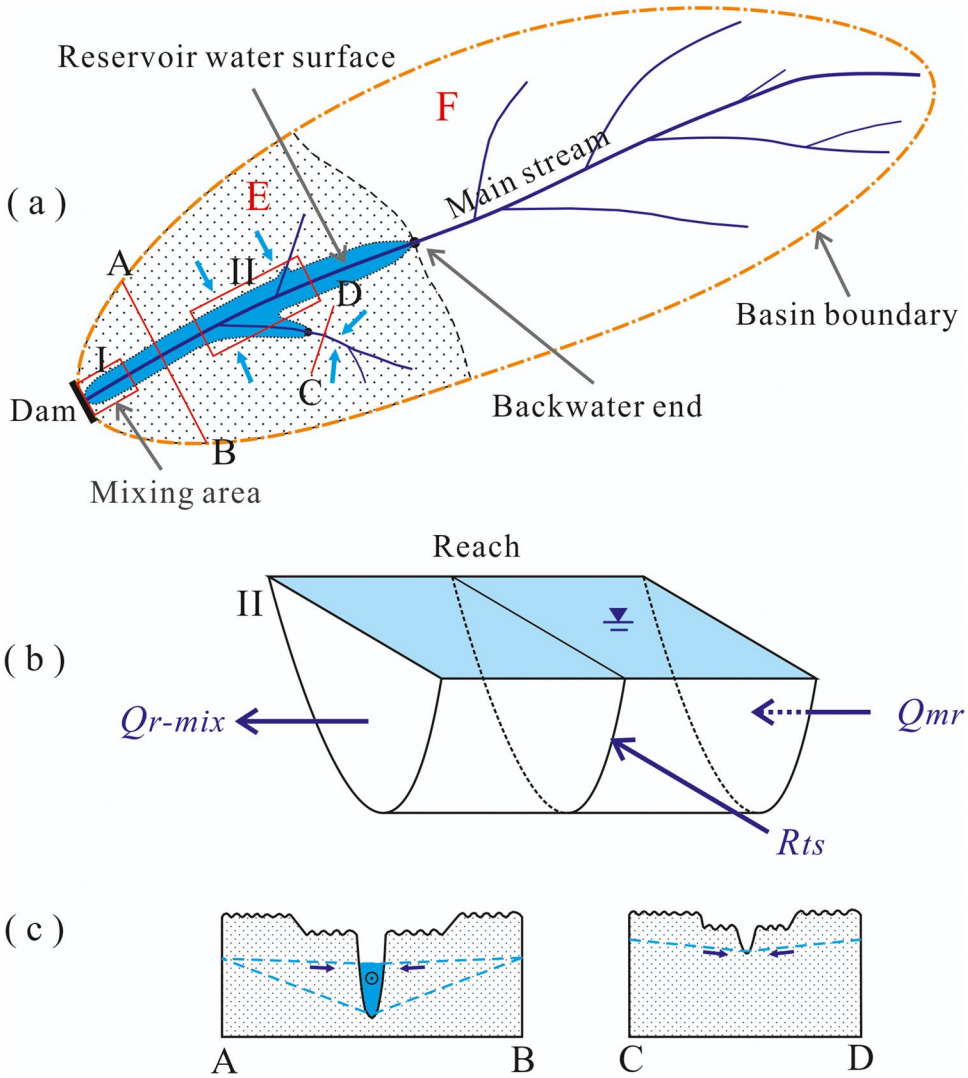


**Fig. 8** Schematic diagram of the water inflow sources in the gorge reservoir. **a** The interval basin (area E) and the upstream backwater basin (area F), divided by the line representing the backwater end of the main stream. **b** The impact of the reservoir backwater on the water sources of a main stream reach. **c** Cross section of the backwater main stream and a tributary not affected by the backwater

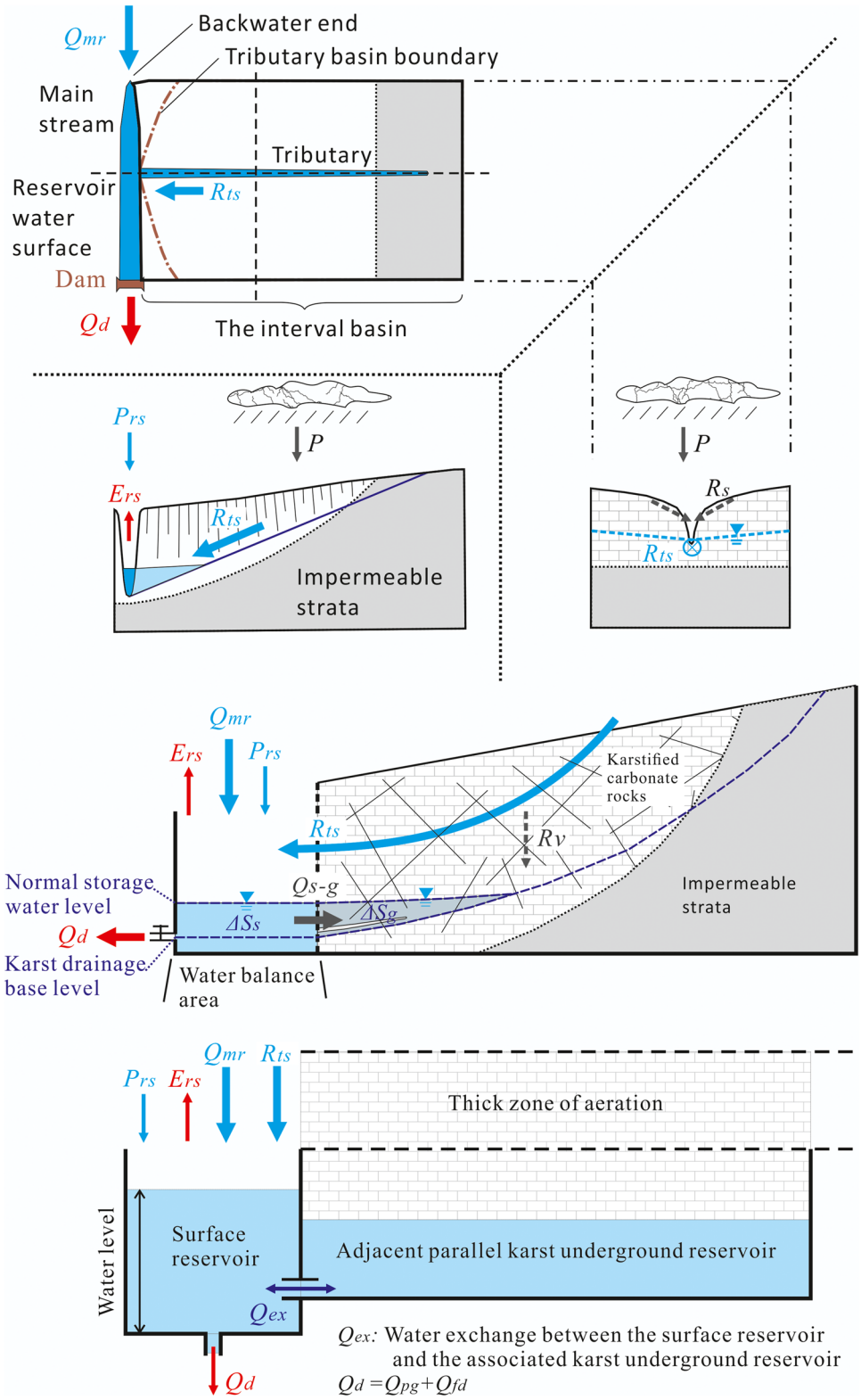


**Fig. 9** Conceptual model of the water balance factors of the Pingzhai Reservoir. $\Delta S_s$ is the water storage change in the surface reservoir, and $\Delta S_g$ is the water storage change in the underground reservoir. The oblique line on the upper part of the karstified carbonate block indicates that the ground surface slope is steep due to the presence of a deeply incised gorge

interval basin of the Pingzhai Reservoir concentrates and flows into the Sancha River rapidly along the gorge tributary network (Fig. 9). Thirdly the horizontal hydraulic conductivity of the karst aquifer beside the Sancha River is far greater than the vertical hydraulic conductivity (Gao 2021). Fourthly, the water surface area of the Pingzhai Reservoir is small, accounting for only 2.6% of the total area of the interval basin from the Yangchang cross section to the dam site

on the main river. As a result, the evapotranspiration from the interval basin changes a little before and after impoundment in the Pingzhai Reservoir (Fig. 5).

According to the aforementioned four hydrogeological characteristics of the study area, a water balance model is proposed to calculate the storage capacity of the karst groundwater reservoir associated with the gorge-type surface reservoir (Fig. 9). In this model, the water-surface area (21 $km^2$) of the Pingzhai Reservoir at a normal water level is taken as the water balance calculation area (Fig. 8a), and the initial water impoundment stage after the completion of the reservoir is taken as the water balance period. This model is based on two assumptions: first, the process of runoff yield and flow concentration in the interval basin is rapid, and most of the lateral inflow ($R_{ts}$) quickly flows into the Pingzhai surface reservoir (Fig. 9); and second, a lateral karst underground reservoir/tank in parallel with the Pingzhai surface reservoir can rapidly absorb excess water from the surface reservoir ($\Delta S_g$, Fig. 9).

The water balance equation in this study is expressed as (the related conceptual model is shown in Fig. 9):

$$\Delta S = \Delta S_s + \Delta S_g \tag{1}$$

$$\Delta S = \int_{t_1}^{t_2} (Q_{in} - Q_{out}) dt \tag{2}$$

$$Q_{in} = Q_{mr} + R_{ts} + P_{rs} \tag{3}$$

$$Q_{out} = Q_{pg} + Q_{fd} + E_{rs} \tag{4}$$

where $\Delta S$ is the total change in the available water resources for the whole Pingzhai surface reservoir and its associated lateral karst underground reservoir ($m^3$), $\Delta S_s$ is the change in the water storage of the surface reservoir ($m^3$), which can be calculated using the reservoir characteristic curve and the reservoir water level (Fig. 10), $\Delta S_g$ is the change in the water storage of the lateral karst underground reservoir associated with the surface reservoir ($m^3$), $Q_{in}$ is the input water rate for the entire reservoir surface area ($m^3/s$), $Q_{out}$ is the net discharge rate of the entire reservoir surface area ($m^3/s$), $t_1$ is the beginning of the water balance period, $t_2$ is the end of the water balance period, $Q_{mr}$ is the inflowing water rate from the main stream at the backwater end of the reservoir ($m^3/s$), $R_{ts}$ is the lateral recharge rate from the interval basin from the Yangchang cross section to the dam site ($m^3/s$), $P_{rs}$ is the precipitation that fell directly onto the reservoir surface (mm/month), $Q_{pg}$ is water discharge rate for water that is used in reservoir power generation processes ($m^3/s$), $Q_{fd}$ is the reservoir flood discharge ($m^3/s$), and $E_{rs}$ is the evaporation from the surface reservoir water (mm/month).

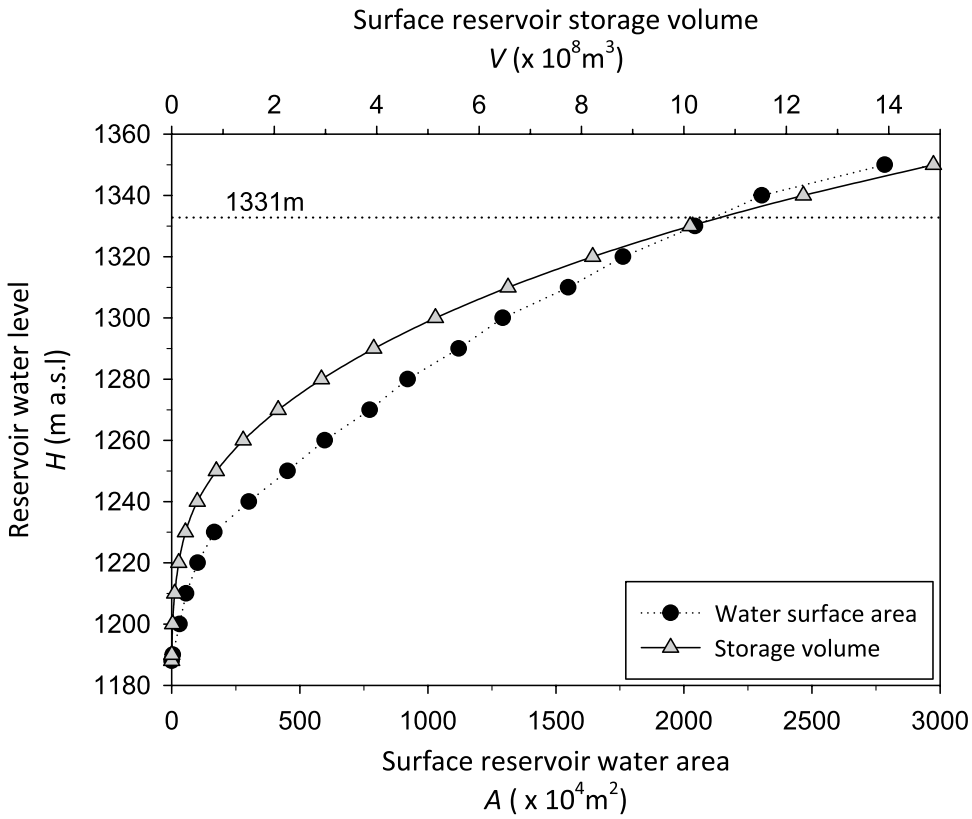


**Fig. 10** Reservoir characteristics (water level vs. water area) curve of the Pingzhai surface reservoir

### Calculation of $R_{ts}$ by artificial neural network

In the initial impoundment stage of the Pingzhai Reservoir after the completion of the concrete-faced rockfill dam, the parameters in the aforementioned Eqs. (3) and (4) were measured directly by the Reservoir Operation Company and the Bureau of Hydrology and Water Resources, except for the $R_{ts}$ parameter. The lateral inflow ($R_{ts}$) from the interval basin of Pingzhai Reservoir is the key to accurately calculate the total input water rate ($Q_{in}$). However, due to the lack of directly observed hydrological data on the lateral inflow before the construction of the Pingzhai Reservoir, it is difficult to establish a conceptual hydrological model that needs to calibrate the parameters through the measured hydrological data, which makes it difficult to calculate the lateral inflow water ($R_{ts}$) from the interval basin using the conceptual hydrological model (Wu 2014; Ma and Liang 2018).

There were no systematic measured hydrological data for $R_{ts}$ in the study area before the construction of the Pingzhai Dam. Fortunately, after the completion of the dam, hydrological observation data such as the surface reservoir water level, rainfall of the interval basin, and discharge rate during the operation of the reservoir were recorded in detail. Considering the aforementioned four hydrogeological characteristics of the study area, a method is proposed to calculate the lateral inflow water from the interval basin of the Pingzhai Reservoir. The first step is to use the measured hydrological data, i.e., the main stream inflow, surface reservoir outflow, rainfall of the interval basin, surface reservoir water level, and reservoir water surface evaporation, during the formal operation period of the Pingzhai Reservoir after its water level had reached the normal storage water level to calculate the monthly lateral inflow from the interval basin using the water balance method. The second step is to establish a nonlinear mapping database between the calculated monthly lateral inflow and the meteorological factors such as rainfall and air temperature. Third, an ANN model is established and trained to simulate the monthly lateral inflow of the interval basin during the operation period of the reservoir. Finally, the monthly lateral inflow of the interval basin during the initial impoundment period of the reservoir is calculated by the preceding trained ANN model (Fig. 11). The preceding method to calculate monthly lateral inflow from the interval basin at the initial stage of reservoir impoundment was mainly based on the following two facts: (1) after the water level of the reservoir reached the normal water level—because the solution cavity and cavern of the karst underground reservoir associated with the surface reservoir had been filled with water, the fluctuation range of the storage water level (26 m) was much smaller than the dam height (162.7 m; Fig. 11), and the regulating capacity of the underground reservoir was low at this time—the calculation error of the monthly lateral inflow from the interval basin in the initial impoundment period was small; (2) before and after the construction of the large dam, although the runoff yield and flow concentration conditions of the interval basin, the flood peak process, and the peak time lag in the river channel will change in a short-term time scale during a flood, the reservoir is a deep canyon reservoir with a small reservoir water surface area, which results in a small change of evapotranspiration in the interval basin. Therefore, in monthly, seasonal, and even annual long-time scales, the changes in the runoff yield and flow concentration conditions of the interval basin have little effect on the total runoff volume (Ye 1992).

For the rainfall-runoff modeling, the black-box hydrological model usually shows more adaptability and superiority than the physical-based and conceptual models (Nourani et al. 2007; Clarke 1994), and can provide more accurate predictions quickly and conveniently. In nonlinear black-box hydrological models of rainfall-runoff simulation, artificial intelligence (AI) technology based on the ANN method has been widely used (Abrahart et al. 2012; Badrzadeh et al. 2015; Nourani 2017; Zeng et al. 2013). Therefore, the ANN approach was used to establish a black-box hydrological model of the monthly rainfall and lateral inflow of the interval basin of Pingzhai Reservoir.

A back-propagation neural network (BP-NN) is an important type of ANN model with self-organizing and self-teaching abilities. BP-NNs are widely used in the simulation of nonlinear hydrological systems. A BP-NN is usually composed of an input layer, several hidden layers, and an output layer, and adopts the back-propagation algorithm to minimize the RMSE between the predicted outputs and the target outputs to train the network (Wang et al. 2000; Chaolun and Jia 2007).

In this study, a three-layer BP-NN with three neurons in the input layer, five neurons in the hidden layer, and one neuron in the output layer was chosen to model the monthly rainfall-runoff process in the Pingzhai Reservoir interval basin. Hyperbolic tangent and linear functions were selected as the activation functions of the hidden layer and output layers, respectively (Wang et al. 2000). From 2017 to 2020, the storage water level of Pingzhai Reservoir reached the normal storage water level. The monthly rainfall and air temperature data during this period were taken as the training dataset of the neural network model. The datasets were normalized to give values between −0.95 and 0.95 prior to training. The learning rate and the momentum factor of the neural network model were set to be 0.05 and 0.9, respectively.

There are two steps in reconstructing the monthly lateral inflow from the interval basin of the Pingzhai Reservoir during the initial impoundment period using the BP-NN model with an architecture of 3-5-1: training and reconstruction (Fig. 11). The first step is the neural network training

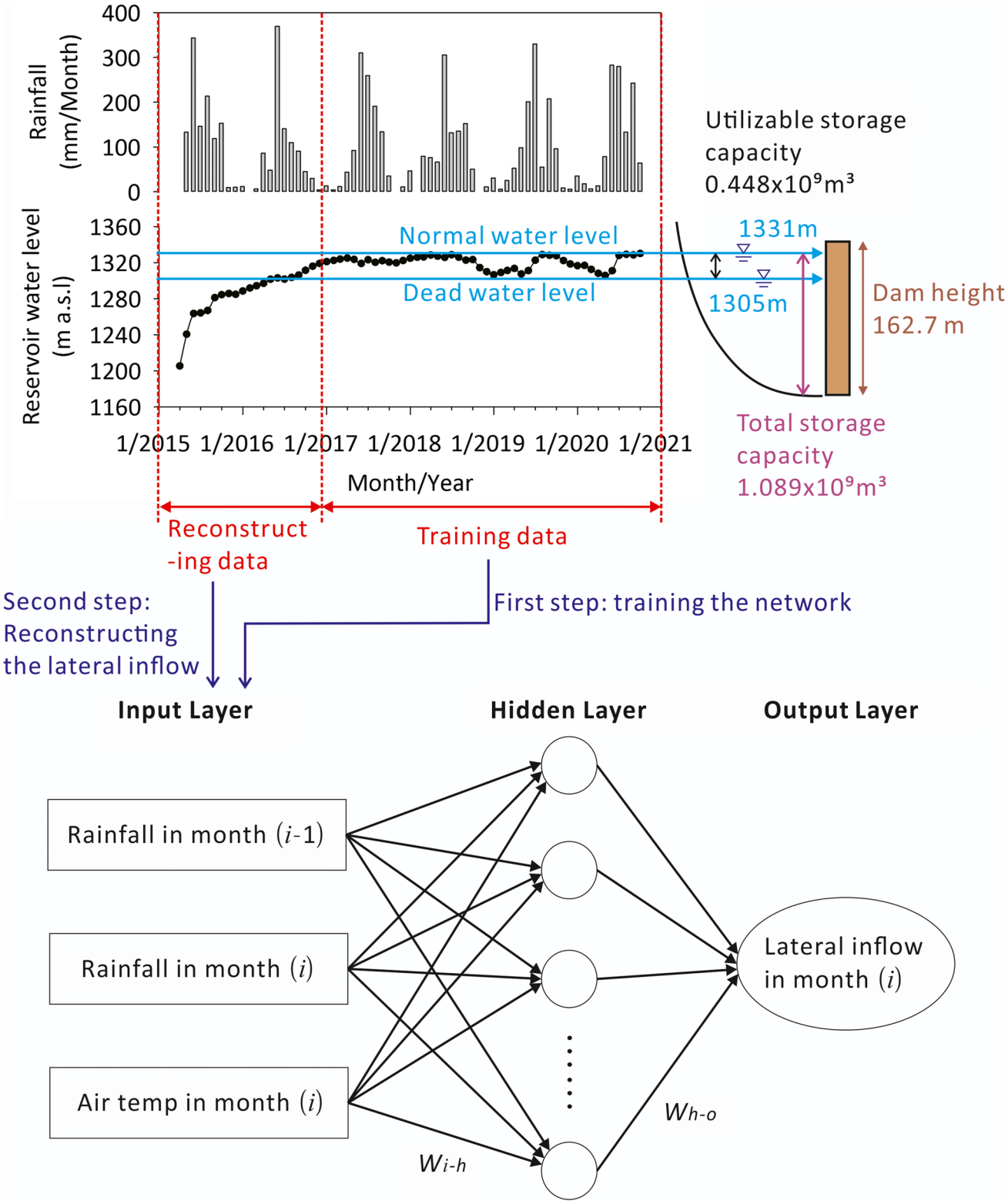


**Fig. 11** Flowchart of the reconstruction process using the back-propagation neural network (BP-NN). $W_{i\text{-}h}$ is the weight from the input layer to the hidden layer, and $W_{h\text{-}o}$ is the weight from the hidden layer to the output layer, and the weights were available from the network training process

process. The nodes of the input layer represent three variables—rainfall in month (*i*-1), rainfall in month (*i*), and air temperature in month (*i*). The output layer nodes represent the dependent variables, i.e., the monthly lateral inflow in month (*i*). The inputs were used to generate monthly lateral inflow, and the BP-NN model was used to simulate the relationship between the inputs and monthly lateral inflow (Fig. 11). Second, the complete time series of the three input variables together with the trained BP-NN model were used to generate a time series of lateral inflow of the interval basin during the initial impoundment period of the Pingzhai Reservoir (Fig. 11).

## Hydrochemical and stable isotopic measurement methods

Hydrochemical and stable isotopic measurements and a two-end-members mixing model were used in the study to assess the reliability of the calculated storage capacity value of the karst underground reservoir with the water balance model. In situ titration was performed in the field and major ion analysis was performed in the laboratory. The stable isotopic measurements were of $\delta^{18}O$ and $\delta^{2}H$. Most of the water samples were collected in each season in 2018. The sampling locations were in the head area of the reservoir, the Yangchang cross section, and the Shuigong River (the largest representative inflowing tributary in the interval basin; Fig. 5).

In the mixing model, the mixing ratio ($V_A/V_B$) of the two water sources is defined as the ratio of the runoff of the main stream at the backwater end of the reservoir during the initial impoundment period ($V_A$) to the lateral runoff of the interval basin between the dam and the backwater end of the main stream ($V_B$). The mixing ratio was then calculated using certain hydrochemical and stable isotopes indices (i.e., the $Cl^-$ concentration and the $\delta^{2}H$ content). Based on the fact that the runoff data from the Yangchang cross section of the main stream are accurate and reliable, the mixing ratios were used to calculate the interval basin area runoff ($\Sigma R_{ts} = V_A/V_B \times \Sigma Q_{mr}$) and assess the reliability of these calculated interval runoff results. Finally, these water balance factors of $R_{ts}$ were substituted into the water balance equation to calculate both the value and the error of the storage capacity of the associated karst underground reservoir.

### In situ titration and major ion analysis in the laboratory and calculation of the saturation index

The carbonate chemistry of karst water is sensitive to environmental conditions, so the physicochemical parameters (i.e., water temperature, pH, and bicarbonate concentration) of the water were measured in situ as soon as the water samples were collected (Fetter 1994). The calcium ($Ca^{2+}$) and bicarbonate ($HCO_3^-$) concentrations of water were titrated in situ with a calcium test kit and an alkalinity test kit made by Merck Company in Germany, with an accuracy of 1 and 0.05 mmol/L, respectively (Zolotov et al. 2002; Banks and Frengstad 2006; Liu et al. 2007). Two sets of 60-ml water samples were transferred in acid-washed hydroplastic bottles for chemical analysis of cations and anions within 2 weeks, after being filtered through 0.45-μm Millipore filters. The cation test samples were acidified to pH < 2.0 with concentrated nitric acid to prevent complexation and precipitation.

In the laboratory (the State Key Laboratory of Environmental Geochemistry, Institute of Geochemistry, Chinese Academy of Sciences), cation concentrations of $Na^+$, $K^+$, $Ca^{2+}$, and $Mg^{2+}$ were determined by ICP optical emission spectrometry. The anion concentrations of $SO_4^{2-}$ and $Cl^-$ were determined by ion chromatography (Dionex ICS-90; Banks and Frengstad 2006).

The calcite and gypsum saturation indices ($SI_c$ and $SI_g$) of the waters were calculated with the geochemical program PHREEQC using the water temperature and pH measured in situ, and concentrations of $Na^+$, $K^+$, $Mg^{2+}$, $Ca^{2+}$, $SO_4^{2-}$, $Cl^-$, and $HCO_3^-$.

### Measurements of stable isotopic compositions of oxygen ($\delta^{18}O$) and hydrogen ($\delta^{2}H$)

Water samples for $\delta^{18}O$ and $\delta^{2}H$ analysis were collected in 60-ml hydroplastic bottles. During the collection process, the bottles were completely filled with water to prevent any evaporation, and then stored in a refrigerator until further analysis. The $\delta^{18}O$ and $\delta^{2}H$ analysis was performed using conventional laser absorption spectroscopy in a liquid-water isotope analyzer (Los Gatos Research, Inc, USA). The $^{18}O/^{16}O$ and $^{2}H/^{1}H$ were expressed in the δ notation as parts/thousand differences (‰) with respect to the Vienna Standard Mean Ocean Water (VSMOW). The accuracy of the $\delta^{18}O$ and $\delta^{2}H$ measurements were 0.1 and 0.3‰ respectively.

## Results

In this section, the measured hydrological data of Pingzhai Reservoir and the calculated lateral inflow of the interval basin using the ANN method in the initial impoundment period were substituted into the water balance model—Fig. 9; Eqs. (1)–(4)—to inversely calculate the total storage capacity of the karst underground reservoir associated with the Pingzhai surface reservoir. The hydrogeochemical data were obtained to assess the reliability of the calculated storage capacity value. The results of this analysis are presented in Figs. 12 and 13 and Tables 1 and 2.

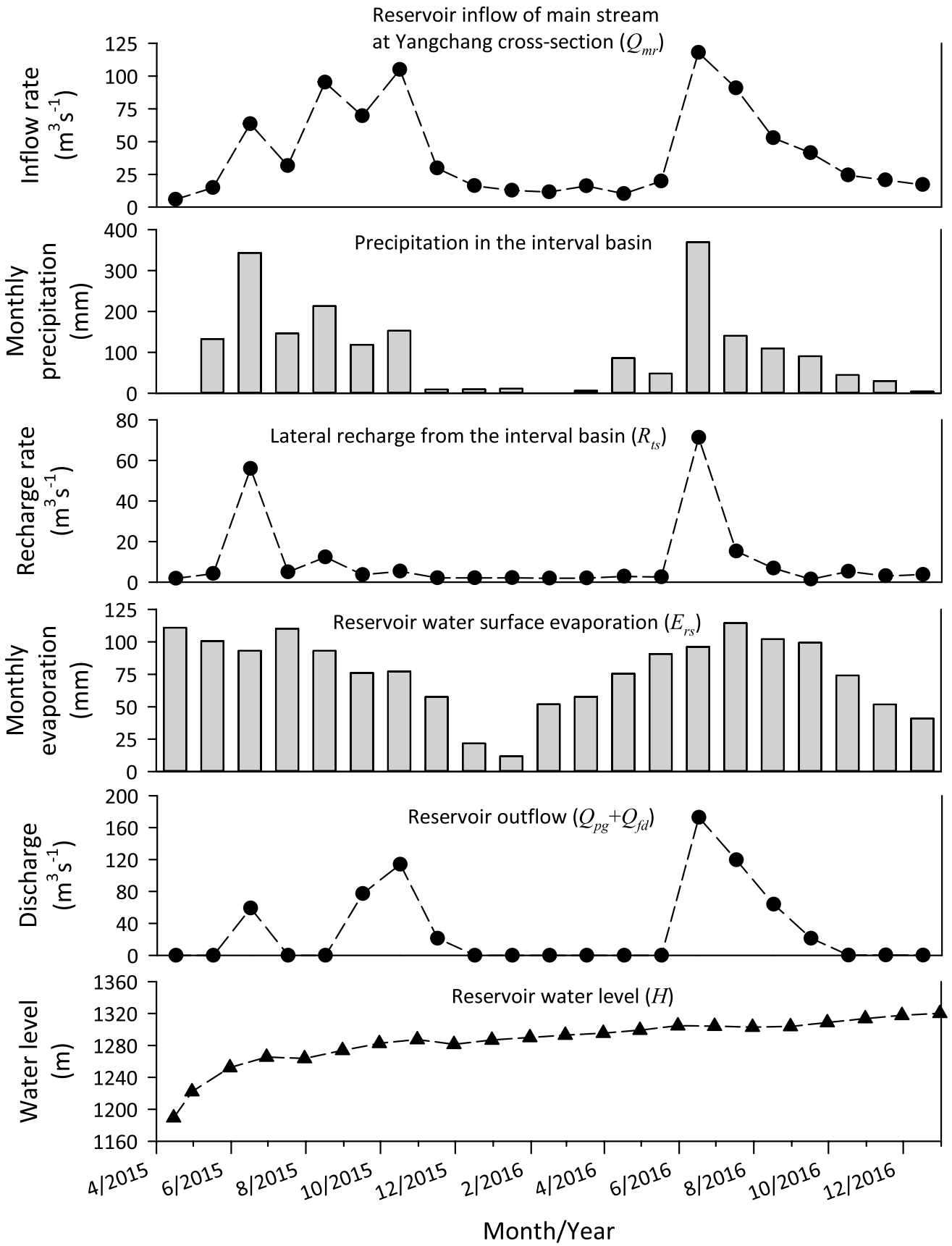


**Fig. 12** Variations in the water balance factors throughout the initial impoundment stage of the Pingzhai Reservoir

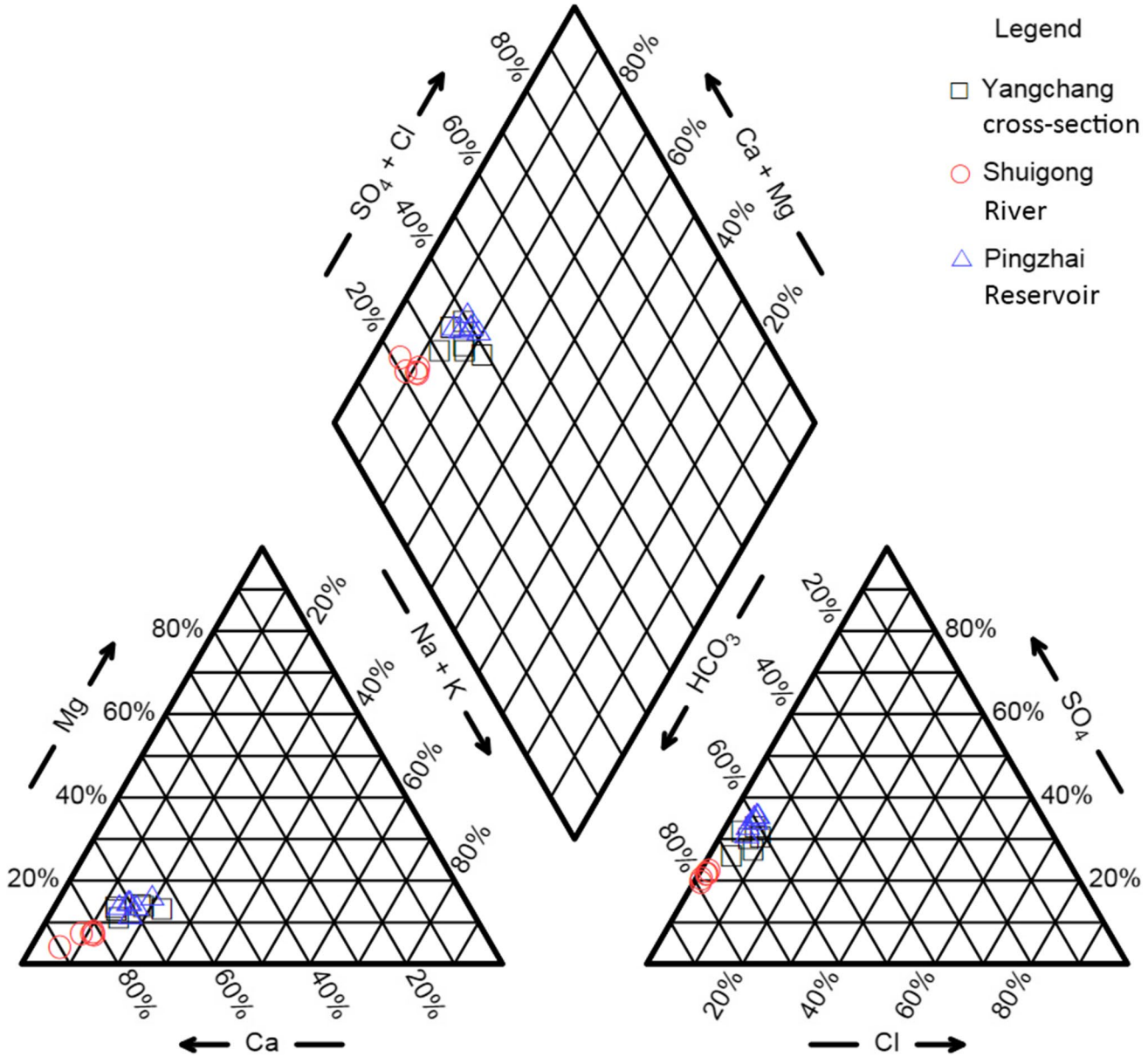


**Fig. 13** Piper diagram of the different water types in the Pingzhai Reservoir basin area

**Table 1** Water balance factors for the initial impoundment period of the Pingzhai Reservoir

| Water balance factors | | Value ($\times 10^9$ m$^3$) |
|---|---|---|
| $\Sigma Q_{in}$ | $\Sigma Q_{mr}$ | 2.286 |
| | $\Sigma R_{ts}$ | 0.555 |
| | $\Sigma P_{rs}$ | 0.021 |
| $\Sigma Q_{out}$ | $\Sigma E_{rs}$ | 0.017 |
| | $\Sigma Q_{pg} + \Sigma Q_{fd}$ | 1.710 |
| $\Delta S_s$ | - | 0.824 |

## Water balance factors and the underground reservoir capacity

The sluice was officially closed in April 2015 after the completion of the Pingzhai Reservoir Dam. The initial impoundment phase continued until the end of December 2016. During the initial impoundment period, researchers carefully recorded the precipitation in the interval basin, the cross-sectional flow of the main stream at the backwater end, the reservoir discharge, and other water balance factors in the

**Table 2** Annual mean physicochemical parameter values in water samples collected within the Pingzhai Reservoir basin

| Item | Unit | Yangchang cross section | Shuigong River | Pingzhai Reservoir |
|---|---|---|---|---|
| Temp | °C | 14.69 | 13.61 | 16.10 |
| pH | - | 8.07 | 8.54 | 7.95 |
| $_{Ca}2+$ | mg/L | 67.00 | 41.00 | 63.17 |
| $_{Mg}2+$ | mg/L | 7.59 | 1.99 | 7.43 |
| $Na^+$ | mg/L | 16.78 | 5.08 | 14.92 |
| $_{K}+$ | mg/L | 2.91 | 0.68 | 2.99 |
| $HCO_3^-$ | mg/L | 177.92 | 111.02 | 148.43 |
| $SO_4^{2-}$ | mg/L | 65.20 | 24.01 | 64.63 |
| $Cl^-$ | mg/L | 9.54 | 1.33 | 7.55 |
| $SI_c$ | - | 0.52 | 0.59 | 0.31 |
| $SI_g$ | - | −1.73 | −2.27 | −1.76 |
| $\gamma Na/\gamma Cl$ | - | 2.58 | 5.81 | 3.06 |
| $\delta^{18}O$ (VSMOW) | ‰ | −9.65 | −9.66 | −9.70 |
| $\delta^{2}H$ (VSMOW) | ‰ | −67.02 | −63.52 | −66.36 |

reservoir basin. With these measured data and the calculated lateral inflow of the interval basin using the ANN method, the water balance method was used to calculate the storage capacity of the underground karst groundwater reservoir that is associated with the Pingzhai surface reservoir.

The water balance period was defined as the initial impoundment stage (from April of 2015 to December of 2016) of the Pingzhai Reservoir. In this time period, the reservoir water level rose from 1,189.4 to 1,320.1 m above sea level (a.s.l.). The water balance area is defined as the reservoir water surface area (an area of 21 $km^2$, accounting for only 2.6% of total area of the interval basin; Fig. 5).

As shown in Fig. 9, the reservoir water surface area input factors include the inflow ($Q_{mr}$) of the Yangchang cross section at the backwater end of the main stream of the reservoir, the lateral recharge ($R_{ts}$) of the interval basin from the Yangchang cross section to the Pingzhai Reservoir dam site, and the precipitation that falls directly onto the water surface of the reservoir ($P_{rs}$). The reservoir output factors include the power generation flow ($Q_{pg}$), the flood discharge flow ($Q_{fd}$), and the water surface evaporation ($E_{rs}$). The storage factors for the surface reservoir and adjacent parallel karst underground reservoir include the surface reservoir storage—$\Delta S_s$, which can be calculated using the reservoir characteristic curve with the measured water level (Fig. 10)—and the groundwater storage ($\Delta S_g$, which is unknown, but can be obtained through the inversion of other balance factors). The data of these water balance factors throughout the initial impoundment period of the reservoir are presented in Fig. 12.

During the water balance period (i.e., the initial impoundment) of the Pingzhai Reservoir, the inflow through the Yangchang cross section at the backwater end of the Sancha River ($\Sigma Q_{mr}$) is $2.286 \times 10^9$ $m^3$, the total interval inflow ($\Sigma R_{ts}$) is $0.555 \times 10^9$ $m^3$, the amount of precipitation that fell directly onto the water surface of the reservoir ($\Sigma P_{rs}$) is $0.021 \times 10^9$ $m^3$, the total water inflow into the reservoir ($\Sigma Q_{in}$) is $2.862 \times 10^9$ $m^3$, the amount of water that evaporated out of the water surface of the reservoir ($\Sigma E_{rs}$) is $0.017 \times 10^9$ $m^3$, the power generation and the flood discharge of the reservoir ($\Sigma Q_{pg} + \Sigma Q_{fd}$) is $1.710 \times 10^9$ $m^3$, the total water output of the reservoir basin ($\Sigma Q_{out}$) is $1.727 \times 10^9$ $m^3$ (Table 1), and the measured water level of Pingzhai Reservoir at the end of December of 2016 was 1,320.1 m. Per the reservoir characteristic curve (Fig. 10), this corresponds to a surface reservoir water storage ($\Delta S_s$) of $0.824 \times 10^9$ $m^3$. Using these known water balance factors, it was determined that the storage capacity change in the underground reservoir (and, therefore, the storage capacity of the karst underground reservoir associated with the Pingzhai surface reservoir) is $0.311 \times 10^9$ $m^3$ (the corresponding storage water level is 1,320.1 m a.s.l.):

$$\begin{aligned}\Delta S_g &= \sum \left[Q_{mr} + R_{ts} + P_{rs} - \left(E_{rs} + Q_{pg} + Q_{fd}\right)\right] - \Delta S_s \\ &= \sum Q_{mr} + \sum R_{ts} + \sum P_{rs} - \sum E_{rs} - \sum Q_{pg} - \sum Q_{fd} - \Delta S \\ &2.286 + 0.555 + 0.021 - (0.017 + 1.710) - 0.824\left(\text{billion} \bullet m^3\right) \\ &= 0.311\left(\text{billion} \bullet m^3\right).\end{aligned} \tag{5}$$

## Hydrogeochemistry and stable isotopes

Water samples were collected from the reservoir head area, the Yangchang cross section, and the Shuigong River (Fig. 5). The main ions and the stable hydrogen and oxygen isotopes were analyzed, and the results are summarized in Table 2. The measured concentrations of the minor ions ($K^+$, $Na^+$, $Mg^{2+}$, $Cl^-$, and $SO_4^{2-}$) and field-titrated contents of the major ions ($Ca^{2+}$ and $HCO_3^-$) of the three water sample

series were plotted on a Piper diagram (Fig. 13). Figure 13 shows that the hydrochemical facies of the three water sample series are all $HCO_3$–Ca type, reflecting the lithological control on the hydrochemical facies. It is still noted, however, that there are small hydrochemical differences. The differences in the ion concentrations and $\delta^{18}O$ and $\delta^{2}H$ values of various types of water provide a basis for verifying the reliability of the calculated value of the capacity of the linked underground reservoir using the mixing equation.

## Discussion

These results provide the calculated storage capacity of the karst underground reservoir associated with Pingzhai Dam, as well as the hydrochemical and isotopic data necessary to evaluate the reliability of this value. The following results enable us to better understand underground reservoirs that are closely linked with large dams in hilly and mountainous karst areas.

### Assessment of the error of the calculated storage capacity of the karst underground reservoir

The storage capacity of the underground reservoir that is closely linked with the Pingzhai Reservoir dam was calculated using the water balance method and is $0.311 \times 10^9$ $m^3$. This represents 29% of the total storage capacity of the surface reservoir. This value is far greater than expected. As noted, except for the lateral inflow ($R_{ts}$) from the interval basin area of the Pingzhai Reservoir, the data for the other water balance factors involved in the calculations were obtained from the hydrological and meteorological monitoring station managed by the Pingzhai Reservoir Authority and Guizhou Hydrology and Water Resources Bureau, and these data have a high quality and reliability. However, the probability of some uncertainty in the calculation of the lateral runoff ($R_{ts}$) in the interval basin between the backwater end of the main stream and the dam site using the ANN method was noted. To quantify this uncertainty, the interval basin area runoff was assessed using hydrogeological, hydrochemistry and isotope techniques. With this information, one can infer how the error in the interval basin runoff may have affected the associated karst underground storage capacity calculation. The storage capacity and macroscopic volumetric karst rate of the karst underground reservoir associated with the surface reservoir in the canyon karst area were examined from the perspective of karstology.

### Estimation of the underground storage capacity via hydrogeological analogy

The drainage area of the main stream of the Sancha River above the Yangchang cross section is 2,677 $km^2$, and the average annual discharge rate of the cross section is 41.97 $m^3/s$ (for a statistical period of 1958–2016). The land surface area of the interval basin between the Yangchang cross section and the dam site is 794 $km^2$. According to basic hydrogeological analogy principles, as long as the climate and hydrogeological conditions do not change drastically, the runoff increases with the basin area (Fang et al. 1996). That is to say, the ratio of $\Sigma Q_{mr}$ to $\Sigma R_{ts}$ during the initial impoundment period of Pingzhai Reservoir is the corresponding drainage area ratio (3.37; Table 3). Therefore, it is estimated that the runoff of the interval basin during the initial impoundment period (21 months in all, from April of 2015 to December of 2016) of the Pingzhai Reservoir is about $0.678 \times 10^9$ $m^3$ (Table 3). By substituting this value into the water balance equation, the reservoir storage capacity of the associated karst underground reservoir was calculated to be $0.434 \times 10^9$ $m^3$ (Table 3).

**Table 3** Underground storage capacity value and uncertainty, as estimated using hydrogeological and hydrogeochemical methods

| Method | Water volume ratio of different end-members, $V_A/V_B$[a] | Runoff of Yangchang cross section (actual measured value) ($10^9$ $m^3$) | Runoff of the interval basin between the dam and the backwater end of the mainstream ($10^9$ $m^3$) | Calculated underground storage capacity values of ($10^9$ $m^3$) | Error magnitude ($10^9$ $m^3$) |
|---|---|---|---|---|---|
| Hydrogeological method | 3.37 | 2.286 | 0.678 | 0.434 | 0.123 |
| $Cl^-$ end-member mixing equation | 3.13 | 2.286 | 0.730 | 0.486 | 0.175 |
| $\delta^2H$ end-member mixing equation | 4.30 | 2.286 | 0.532 | 0.288 | −0.023 |
| Hydrometry | – | 2.286 | 0.555 | 0.311 | -- |

[a]*A*: inflow from the main stream at the backwater end of the Pingzhai Reservoir. *B*: inflow of the interval basin from Yangchang cross section to the dam site

### Estimation of the underground storage capacity using the hydrochemical and stable isotopic two-end-member mixing model

Hydrochemical techniques provide significant information about the functioning of karst aquifer systems, and they complement hydrodynamic methods (Goldscheider and Drew 2007). A two-end-member mixing model with hydrochemical and stable isotopic data was used in this study to assess the reliability of the storage capacity of the karst underground reservoir calculated using the water balance model.

In general, the water in the Pingzhai Reservoir is mainly a mixture of water from the main stream at the end of the backwater region (area F in Fig. 8a) and water from the interval basin (area E in Fig. 8a). Because the water surface area of the Pingzhai Reservoir is far less than the land surface area of the interval basin, the influence of the atmospheric rainfall that falls directly onto the reservoir water surface on the geochemistry of the reservoir water is minimal. This observation is based on the fact that the Pingzhai Reservoir is located in a deep gorge that has been down-cut by the main stream of the Sancha River and that the backwater reach of the main stream extends for a significant distance along the upstream direction. The water in an impoundment reach mainly comes from the river water in the upper main stream ($Q_{mr}$) and the lateral inflow water of the interval basin ($R_{ts}$) (Fig. 8b). Because the reservoir water spends a considerable amount of time in the long narrow canyon, the two water sources mix as the water flows towards the dam, resulting in water that is evenly mixed by the time the water makes its way to the reservoir head (area I near the dam in Fig. 8a). The river water in the main tributary of the reservoir interval area takes on the hydrochemical and isotopic characteristics of the lateral inflow water from the interval basin surface. Based on this mixing model, the hydrochemistry and isotope data from the main stream inflow at the end of the reservoir backwater and the interval basin inflow were used to calculate the mixing ratio of the water in the Pingzhai Reservoir. The results of these hydrogeochemical analyses are presented in Table 2 and Fig. 13.

As shown in Fig. 13, the water from the main stream at the backwater end of the reservoir, the water from the Shuigong River at the interval basin, and the mixed reservoir water are all characterized by high $HCO_3$–Ca contents. The saturation index of calcite in these three kinds of water is larger than zero, indicating that the calcite in the water is in a supersaturated state (Table 2). That is, because $Ca^{2+}$ and $HCO_3^-$ are nonconservative chemical components that may precipitate out as calcite, it is not appropriate to use these components in the mixing ratio calculation for the two water end-members. The $Na^+$, $SO_4^{2-}$, and $K^+$ components are also not conserved because of the cation exchange adsorption reaction, the adsorption of hydroxides in the sediments of humid subtropical zones and the reduction of hydroxides under anoxic conditions, and the effect of plant uptake, respectively. The $Cl^-$ ion is

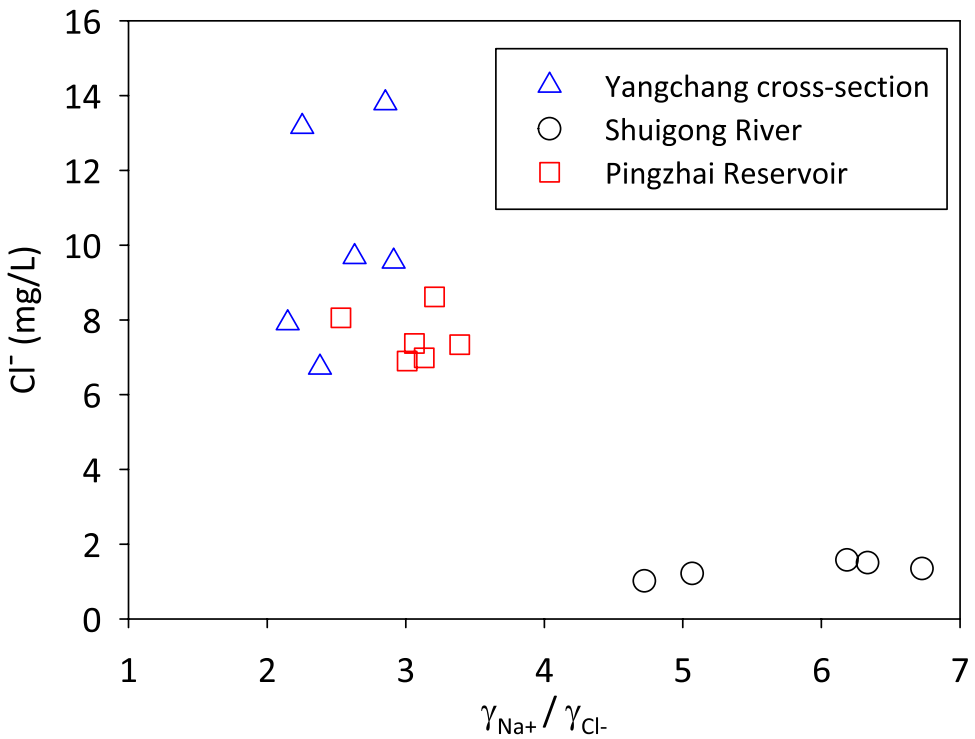


**Fig. 14** Plot of the chloride concentration and the Na/Cl equivalent ratio for the various water types in the Pingzhai Reservoir basin area

conserved because it is unlikely to form insoluble minerals in water with low salinity values, it is not adsorbed by colloids, and it is not typically absorbed by organisms. As such, the two end-members of the mixed water model were determined using the $Cl^-$ concentration (Ovchenikov 1958). As shown in Fig. 14, the two end-members of the Pingzhai Reservoir inflows are distinctly different in their $Cl^-$ concentrations and their $\gamma_{Na}/\gamma_{Cl}$ equivalent ratios. Using the $Cl^-$ concentration, one can calculate the mixing ratio for the two end-members:

$$\frac{V_A}{V_B} = \frac{Y_{mix} - S_B}{S_A - Y_{mix}} \tag{6}$$

where $V_A$ is the volume of water A (the water from the main stream at the backwater end of the reservoir), $V_B$ is the volume of water B (the water from the interval basin of Pingzhai Reservoir), $S_A$ is the concentration of a conservative component in water A, $S_B$ is the concentration of the conservative component in water B, and $Y_{mix}$ is the concentration of the conservative component in the mixed water.

Table 2 shows the chloride concentration of the two end-members (i.e., the Yangchang cross section and the Shuigong River) and the mixed reservoir water. The values of $S_A$, $S_B$, and $Y_{mix}$ are 9.54, 1.33, and 7.55, respectively, and the mixing ratio $V_A/V_B$ is 3.13 (Table 3). Using this mixing ratio, the $Q_{mr}$ data, which have high reliability, directly measured at the hydrological station at Yangchang cross section can be converted into the lateral inflow from the interval basin. Then, the storage capacity of the associated karst underground reservoir can be calculated using the water balance equation. The underground reservoir capacity is $0.486 \times 10^9$ $m^3$.

Hydrogen and oxygen stable isotopes are also used to independently determine the mixing ratio (Clark and Fritz 1997). In the Pingzhai Reservoir area, the amount of stable oxygen isotopes in different water sources ranges from −10.52 to −8.91‰ with an interval length of 1.60‰ and the stable hydrogen isotope content ranges from −68.91 to −60.99‰ with an interval length of 7.91‰. Here, one divides the test accuracy of the hydrogen and oxygen isotopes by their respective interval lengths and defines this new quotient as the relative accuracy. The results show that the relative oxygen isotope accuracy and the relative hydrogen isotope accuracy are 0.062 and 0.025, respectively. As such, it is concluded that the hydrogen isotope results are more accurate than those of the oxygen isotopes and use the hydrogen isotope data (VSMOW) to calculate the end-member mixing ratio of the water in the Pingzhai Reservoir.

If the stable isotopic compositions of water samples A and B are $\delta_A$ and $\delta_B$, respectively, and if the isotopic composition of the mixed water is $\delta_{mix}$, then the mixing ratio can be expressed as:

$$\frac{V_A}{V_B} = \frac{\delta_{mix} - \delta_B}{\delta_A - \delta_{mix}} \tag{7}$$

where $V_A$ is the volume of water A (the water from the main stream at the backwater end of the reservoir), $V_B$ is the volume of water B (the water from the interval basin of Pingzhai Reservoir), $\delta_A$ is the isotope content of water A, $\delta_B$ is the isotope content of water B, and $\delta_{mix}$ is the isotope content of the mixed water.

Table 2 shows the isotope values of the two-end-member water types and the mixed reservoir water. The values of $\delta_A$, $\delta_B$, and $\delta_{mix}$ are −67.0, −63.5, and −66.4‰, respectively, and the mixing ratio $V_A/V_B$ is 4.30 (Table 3). Using this mixing ratio, the $Q_{mr}$ data can be converted into the lateral inflow from the interval basin, and then, the storage capacity of the associated karst underground reservoir ($0.486 \times 10^9$ $m^3$) can be calculated using the water balance equation.

### The uncertainty of the capacity of the underground reservoir, calculated from the perspective of the volumetric karst rate

The results of the uncertainty analysis of the calculated capacity of the associated underground reservoir showed that the hydrogeological area analogy method ($0.678 \times 10^9$ $m^3$), the chloride concentration method ($0.730 \times 10^9$ $m^3$), and the hydrogen stable isotope method ($0.532 \times 10^9$ $m^3$) all produce relatively similar estimates of the interval basin runoff (Table 3). These interval basin runoff values were then substituted into the water balance equation (where the interval basin runoff is the only source of error) to determine the uncertainty of the storage capacity of the karst underground reservoir. Based on this analysis, the maximum storage capacity of the karst underground reservoir is $0.486 \times 10^9$ $m^3$, the minimum storage capacity is $0.288 \times 10^9$ $m^3$, and the standard deviation of the storage capacity is $\pm 0.108 \times 10^9$ $m^3$ (Table 3).

In addition, the karstification rate also can be used to assess the reliability of the calculated karst underground reservoir capability. The karstification rate (i.e., the karst rate or karst porosity, expressed as a percentage) is one method of assessing the degree of karst development in a given area. There are three types of karst rates: the linear karst rate (e.g., drilling boreholes), the areal karst rate, and the volumetric karst rate (Lu 2001; Zeng et al. 2020). The areal karst rate is defined as the ratio of the area of the cavern slices to the total area of a carbonate plane (often determined in a full-azimuthal three-dimensional seismic survey), and the volumetric karst rate refers to

the percentage of the volume of karst cavities per unit volume. These three karst rates are respectively utilized at the microscopic (e.g., hand specimen), mesoscopic (e.g., pumping test), and macroscopic (e.g., regional) scales (Ford and Williams 2007). While the volumetric karst rate for a given region is an important parameter in karst water resources assessments, it is often difficult to quantify. In this study, geographic information system (GIS) software was used to reconstruct the fold morphology of the Lower Triassic Yongningzhen Formation limestone in the Pingzhai Reservoir basin (Figs. 6 and 7). After analyzing the riverbed profiles of the main surface rivers, it was found that the main rivers in the Pingzhai Reservoir area, as the base level of karst erosion, are all located in two synclinal water storage structures composed of Lower Triassic Yongningzhen Formation limestone. The longitudinal sections of their riverbeds are simple oblique lines, and there are no obvious river knick points in the submerged area of the reservoir (Fig. 15). According to the conceptual model of the karst underground reservoir, which is characterized by an inverted cone with an irregular flat base (Fig. 15), a reservoir storage level of 1,320.1 m a.s.l. corresponds to a submerged base plate area of 139.1 $km^2$ in the Lower Triassic Yongningzhen Formation limestone aquifer (Fig. 6). With a water level change of 130.7 m (from 1,189.4 to 1,320.1 m), one can calculate the volume of aquifer:

$$V = \frac{1}{3} \bullet S \bullet h \tag{8}$$

Per Eq. 8, the volume of the aquifer is $6.246 \times 10^9$ $m^3$. By dividing the total storage capacity of the karst underground reservoir by the volume of the saturated karst aquifer, a macroscopic volumetric karst rate of 0.050 was calculated; this value is consistent with the reported karst rates of other parts of the karst area in southern China (Lu 2001). Because the macroscopic volumetric karst rate is reasonable, it was concluded that the calculated underground reservoir capacity is also reasonable.

## Discussion of karst underground reservoir capacity calculation

In the previous construction of large dams, the site selection of the dam generally involved avoiding carbonate areas with strong karstification. The main reason for this selection is that it is difficult to solve the problem of reservoir leakage caused by the karst conduit. With the increasing development and improvement of geophysical exploration and the hanging curtain grouting technique, Wujiangdu Dam, China's first large concrete dam built on karst strata, was constructed in Guizhou Province in 1983 (Song and Qi 1992; Ma et al. 2005). Since then, Chinese experts in karst

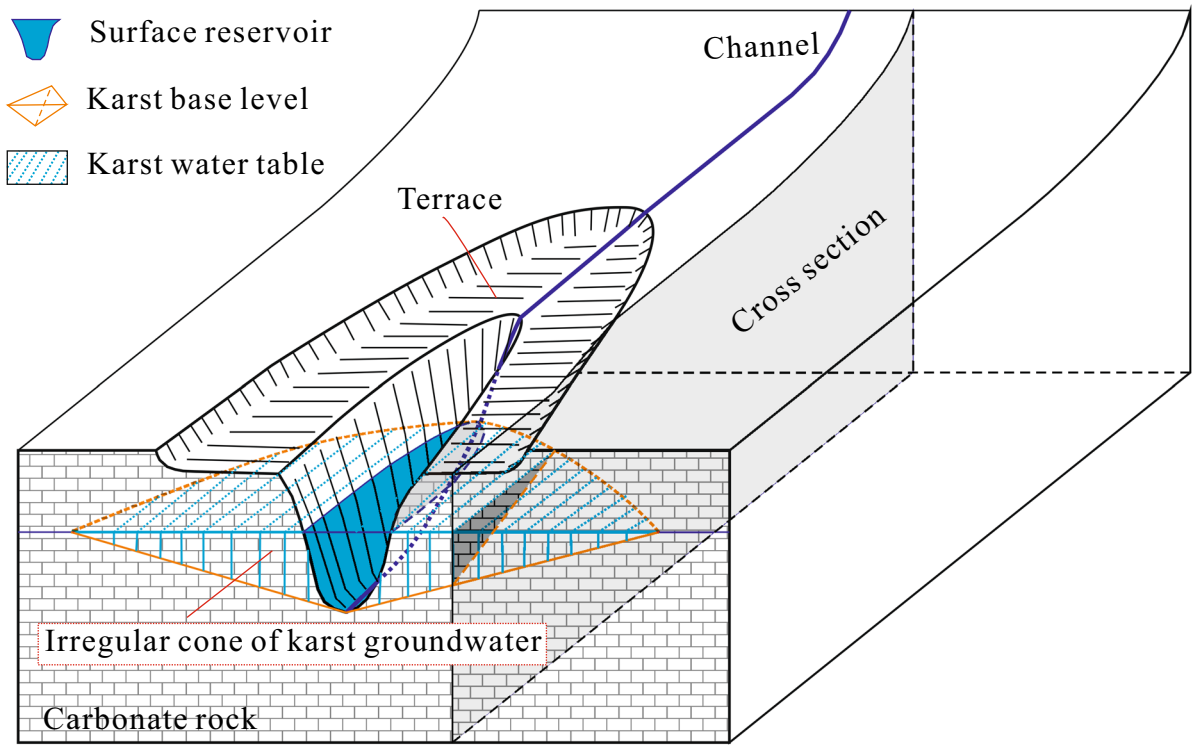


**Fig. 15** Schematic model of an irregular conical underground reservoir associated with a surface reservoir in a deep canyon karst area

hydrogeology and engineering geology have increasingly deepened understanding of karst development and reservoir leakage at dam sites in carbonate areas. Many groundwater reservoirs have been constructed in karst areas in southern and northern China.

Some of the small groundwater reservoirs in the karst area of southern China include the Maguan (Wang 1999), Changgang (Wei and Yang 1997; Chen et al. 1996), and Huanghou (Li et al. 2004) groundwater reservoirs in Guizhou Province and the Xiaopingyang underground reservoir in Guangxi Province (Chen and Zhang 1999). The groundwater reservoirs in the karst area in northern China include the Zhangfang underground reservoir in Beijing (Li 2012) and the Fujiaqiao underground reservoir near the Laiwu Iron and Steel Factory in Shangdong Province (Deng 2004). Although significant advancements have been made in the curtain grouting technique, some problems remain, one of which is the effective determination of the storage capacity of the karst underground reservoir.

Based on how the water is stored, karst groundwater reservoirs can be classified as either pure underground reservoirs or joint surface-underground reservoirs (Fig. 16; Deng 1995). Depending on the characteristics of the groundwater aquifer medium, karst underground reservoirs can be further classified as homogeneous, karst cave, or heterogeneous reservoirs (Fig. 16; Deng 1995). Joint surface-underground reservoirs are further classified based on whether the expression of the surficial part of the reservoir is a karst depression, basin (polje), or valley (Deng 1995). For joint surface-underground reservoirs, the dams can be built either underground or on the surface. The complex structure of the karst aquifer medium and the various surface karst landforms, however, create significant challenges in the ability to accurately evaluate the underground storage capacity.

Historically, it has been difficult to calculate the storage capacity of karst underground reservoirs because they are not visible at the surface (Chen et al. 1996). Some techniques that have been used to assess the storage capacities of karst underground reservoirs in the karst areas in southern China include the karst cave geometric generalization method, the water tank simulation method, the lumped model parameter estimation method, the cumulative karst groundwater contour and area method, the multiplication of the karst aquifer volume by the average degree of karstification method, and the karst subterranean river system volume accumulation method (Chen et al. 1996; Gu and Yan 2006; Qian 2010). Because of the complexity of the karst systems in southern China and the limited accuracy of hydrogeological surveys, it has been difficult to determine the storage capacity of a karst underground reservoir before the construction of a water conservancy project (Chen et al. 1996; Qian 2010). At present, the most effective method to assess the storage capacity of a small karst underground reservoir is to conduct underground reservoir discharge tests and use the water balance equation to calculate the storage capacity of the reservoir during a certain operation period. For karst underground reservoirs associated with large dams in carbonate gorge areas; however, it is not feasible to conduct discharge tests because of the high cost. The methodology proposed in this study—that is, using the water balance method in the

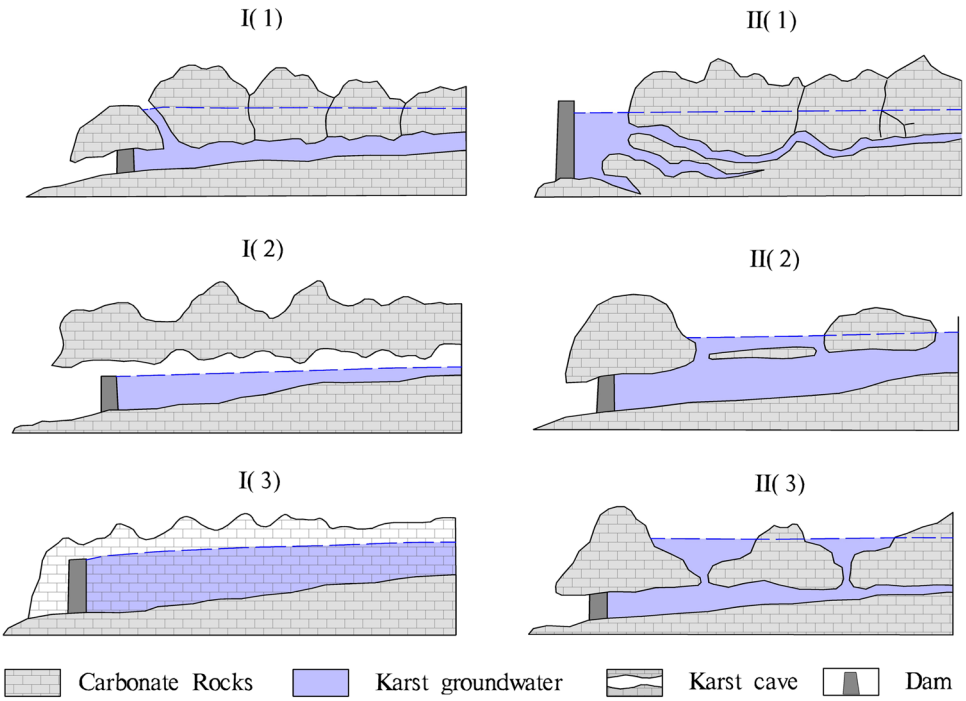


**Fig. 16** Classification of karst underground reservoirs—I(1): underground reservoir with water stored in heterogeneous karst caverns; I(2): underground reservoir with water stored in karst caverns in a subterranean river; I(3): underground reservoir with water stored in homogeneous karst underground cavities; II(1): joint surface and underground reservoir with water stored in an underground reservoir basin and a surface valley; II(2): joint surface and underground reservoir with water stored in an underground reservoir basin and a karst basin; and II(3): joint surface and underground reservoir with water stored in an underground reservoir basin and a karst depression

initial impoundment stage to estimate the storage capacity of a karst underground reservoir closely linked with a large dam—is feasible and effective.

## Implications for research directions in applied karstology

### Implications for water resource development in karst valley areas

The results indicate that in the construction and operation of large dams in hilly and mountainous karst areas, the associated karst underground reservoirs can increase the water supply to the surface reservoirs, improve the stability of the water supply, and increase flood storage. It is necessary to evaluate the storage capacity of the karst underground reservoirs to achieve better joint management of the surface reservoir and the associated underground reservoir. The construction of a large dam in a karst gorge area typically results in the creation of both a surface reservoir and a closely linked underground reservoir (Fig. 9). The surface reservoir is created by river water, which feeds into and ultimately covers the gorge; the storage capacity of the surface reservoir can be directly calculated using the water level, the reservoir geometry, and the volume relationship expressed by the reservoir characteristic curve. Because the water in an underground reservoir is stored in the dissolved pores, fractures, and karst caves in carbonate rocks (Figs. 16 and 3e), it is difficult to observe or directly calculate the storage capacity of such subterranean reservoirs. In fact, the storage capacity of underground water reservoirs is often ignored or regarded as an error in traditional hydrological calculations (Liu and Feng 2002). After the construction of a large surface dam in a karst canyon, the water conservancy department responsible for the operation of the surface reservoir often ignores the existence of the associated underground reservoir and treats the impact of the underground reservoir on the water balance of the entire reservoir region as a water quantity error that arises during the initial impoundment and the operation periods of the surface reservoir. As expected, the existence of this error results in a distinct water imbalance in the floodwater control during the initial impoundment period. Therefore, the underground storage capacity is often not reported (or reported as a water error) and has been largely ignored by hydrologists and hydrogeologists.

This study provides an economically feasible and simple method for calculating the storage capacity of an associated karst underground reservoir and provides basic data for improving the understanding of karst development. Liu and Feng (2002) noted that one of the only ways to obtain a relatively reasonable estimate of the storage capacity of an underground reservoir is to assess the water balance during the initial impoundment period after the completion of a large dam and in the progression of the floodwater through the reservoir during a period in which the reservoir is operational. The application of the water balance method is fairly straightforward. By accounting for the balance factors present during the initial impoundment period of the reservoir, it is possible to quickly and accurately calculate the total storage capacity of a karst underground reservoir.

### Implication for epigenetic paleokarst oil reservoir exploration in petroleum geology

Another important finding of these results is that they provide karst parameters and geological models for the reserve evaluation of epigenetic karst carbonate oil reservoirs in petroleum geology. The characteristics of modern karst are key to understanding paleokarst. In the exploration and development of fractured-vuggy carbonate oil reservoirs formed under an ancient humid tropical or subtropical climate, it is necessary to take a large number of modern karst hydrogeological research results as references. The Tahe Oilfield, a world-famous super-large oilfield, located in the northern margin of the Tarim Basin in northwestern China, has a paleokarst landscape characterized by a fractured-vuggy carbonate reservoir with burial depths of more than 6,000 m, which is similar to that of the modern deep-cut canyon karst area of the Sancha River in Guizhou (Zeng et al. 2020; Li et al. 2016, 2017). The macroscopic volumetric karst rate and the storage capacity of the riverside carbonate blocks along the Pingzhai deep canyon estimated in this study provide direct data support for the reserve evaluation of oil reservoirs with a similar paleo-geomorphology.

## Conclusions

In this study, a water balance inverse algorithm was used, for the first time, in combination with a back-propagation ANN to estimate the storage capacity of the underground reservoir associated with the large Pingzhai Reservoir dam, in the central, subtropical, hilly, and mountainous karst area in southwestern China. The results show that a karst underground reservoir with a storage capacity of $0.311 \times 10^9$ m$^3$ was formed in the karstified carbonate blocks on both sides of the deep Sancha River Valley after the construction of the large Pingzhai Reservoir dam. The underground storage capacity represents 29% of the original total surface storage capacity of the Pingzhai Reservoir dam. These results are supported by hydrochemical and isotopic data. The macroscopic volumetric karst rate of the carbonate blocks on both sides of the deep canyon is 0.050. This result suggests that the storage capacity of underground reservoirs expanded by the surface reservoirs cannot be ignored when large dams are built on deep-cutting rivers in karst hills and mountains.

The results of this study can be used as a reference for the joint management of surface reservoirs and their associated underground reservoirs. Moreover, the regional volumetric karst rate obtained in this study can be used to calculate the oil reserves in deep-cut canyon-type paleokarst reservoirs.

This study, however, does contain some limitations. The main weakness is that because of the characteristics of the hydrogeological survey of the water conservancy and hydropower project, the geological survey data (especially the drilling data) are concentrated in the dam site area of the Pingzhai Reservoir, and relatively little data are available for the interval basin. In the future, the hydrogeological investigation in this area should be strengthened.

**Acknowledgements** We gratefully thank Professor Shijie Wang of the State Key Laboratory of Environmental Geochemistry, Institute of Geochemistry, Chinese Academy of Sciences, China; Professor Dequan Zhou of School of Geography & Environmental Science, Guizhou Normal University, China; Senior Engineer Zuoxiao Li of Guizhou Water Resources Investment (Group) Limited Company, China; Professor Zhiwei Yan and Professor Chunqing Guo of the College of Environmental Science and Engineering, Guilin University of Technology, China; and Senior Engineer Deyong Hu of the 105th Geological Service Company of the Guizhou Bureau of Geology, Mineral Exploration and Development for their thoughtful suggestions, which greatly improved the original draft of the manuscript.

**Funding** This research was supported by the National Natural Science Foundation of China (U1612441, 41673129), the National Key R & D Program of China (2016YFC0502300), and the Science and Technology Foundation of Guizhou Province (SY(2013)3163).

## References

Abrahart RJ, Anctil F, Coulibaly P, Dawson CW, Mount NJ, See LM, Shamseldin AY, Solomatine DP, Toth E, Wilby RL (2012) Two decades of anarchy? Emerging themes and outstanding challenges for neural network river forecasting. Prog Phys Geogr 36:480–513

Badrzadeh H, Sarukkalige R, Jayawardena AW (2015) Hourly runoff forecasting for flood risk management: application of various computational intelligence models. J Hydrol 529:1633–1643. https://doi.org/10.1016/j.jhydrol.2015.07.057

Bakalowicz M (2005) Karst groundwater: a challenge for new resources. Hydrogeol J 13(1):148–160

Banks D, Frengstad B (2006) Evolution of groundwater chemical composition by plagioclase hydrolysis in Norwegian anorthosites. Geochim Cosmochim Acta 70(6):1337–1355. https://doi.org/10.1016/j.gca.2005.11.025

Chaolun BG, Jia DB (2007) Numerical calculation method (in Chinese). China Water & Power Press, Beijing, pp 289–297

Chen DR, Han XR, Luo WQ, Li WX (1996) A preliminary study on storage capacity evaluation for underground reservoir in karst area: taking Changgang Chushuidong underground river in Guizhou Province as an example (in Chinese with English abstract). Carsolog Sin 15(1–2):150–156 (in English with Chinese abstract)

Chen WH, Zhang ZG (1999) The characteristics and regulative capacity of karst aquifers in peak forest and plain area (in Chinese with English abstract). Carsolog Sin 18(1):19–25

Chen Z, Goldscheider N, Auler AS, Bakalowicz M, Broda S, Drew D, Hartmann J, Jiang G, Moosdorf N, Richts A, Stevanovic Z, Veni G, Dumont A, Aureli A, Clos P, Krombholz M (2017a) World karst aquifer map (WHYMAP WOKAM). BGR, IAH, KIT, UNESCO. https://doi.org/10.25928/b2.21_sfkq-r406

Chen Z, Auler AS, Bakalowicz M, Drew D, Griger F, Hartmann J, Jiang G, Moosdorf N, Richts A, Stevanović Z, Veni G, Goldscheider N (2017b) The world karst aquifer mapping project concept, mapping procedure and map of Europe. Hydrogeol J 25(3):771–785

Christensen JH, Hewitson B, Busuioc A, Chen A, Gao X, Held I, Jones R, Kolli RK, Kwon W-T, Laprise R, Magaña Rueda V, Mearns L, Menéndez CG, Räisänen J, Rinke A, Sarr A, Whetton P (2007) Regional climate projections. In: Climate Change 2007: the physical science basis. Contribution of Working Group I to the Fourth Assessment Report of the Intergovernmental Panel on Climate Change, Cambridge University Press, Cambridge

Clark ID, Fritz P (1997) Environmental isotopes in hydrogeology. Lewis, Roca Raton, FL, 312 pp

Clarke RT (1994) Statistical modelling in hydrology. Wiley, Chichester, UK, 412 pp

Deng JC (2004) Study the possibility of building the underground karst reservoir in the Fujiaqiao Karst Area (in Chinese with English abstract). MSc Thesis, Ocean University of China, Qingdao, China, 64 pp

Deng ZM (1995) Factors for building underground reservoir in karst area (in Chinese with English abstract). Guizhou Sci 13(3):16–22

Du XQ, Li YG, Ye XY (2008) Study on concept, types and grades of groundwater reservoir (in Chinese with English abstract). Chin J Underground Space Eng 4(2):209–214

Fang PX, Wei ZD, Liao ZS (1996) Special hydrogeology (in Chinese). Geological Publishing House, Beijing, China, pp 231–234

Fetter CW (1994) Applied hydrogeology. Macmillan College, New York, pp 401–407

Ford D, Williams P (2007) Karst hydrogeology and geomorphology. Wiley, Chichester, UK, 562 pp

Gao H (2021) Numerical Simulation of karst groundwater and analysis of groundwater reservoir capacity in Pingzhai Reservoir Area, Guizhou, China (in Chinese with short English abstract). MSc Thesis, China University of Geosciences, Beijing, 68 pp

Goldscheider N, Drew D (2007) Methods in karst hydrogeology. Taylor and Francis, London

Goldscheider N, Chen Z, Auler AS, Bakalowicz M, Broda S, Drew D, Hartmann J, Jiang G, Moosdorf N, Stevanovic Z, Veni G (2020) Global distribution of carbonate rocks and karst water resources. Hydrogeol J 28:1661–1677. https://doi.org/10.1007/s10040-020-02139-5

Gomes JLS, Vieira FP, Hamza VM (2018) Use of electrical resistivity tomography in selection of sites for underground dams in a semiarid region in southeastern Brazil. Groundw Sustain Dev 7:232–238. https://doi.org/10.1016/j.gsd.2018.06.001

Gu SY, Yan GQ (2006) Karst underground reservoir study in Guizhou Province: review and prospect (in Chinese with English abstract). Guizhou Science 24(1):28–31

Jiang ZC, Yuan DX, Cao JH, Qin XQ, He SY, Zhang C (2012) A study of carbon sink capacity of karst processes in China (in Chinese with English abstract). Acta Geosci Sin 33(2):129–134

Kharazi P, Yazdani MR, Khazealpour P (2019) Suitable identification of underground dam locations, using decision-making methods in a semi-arid region of Iranian Semnan Plain. Groundw Sustain Dev 9:1–10. https://doi.org/10.1016/j.gsd.2019.100240

Li JY, Zuo SY, Fan TZ, Yan GQ (2004) Development and optimal scheduling of karst groundwater resources in mountain area in southern Dushan County (in Chinese). Guizhou Water Power 18(2):35–39

Li SJ (2012) A Study of the characteristics and regulation-storage capacity of the Zhangfang karst-groundwater reservoir in Beijing (in Chinese with English abstract). PhD Thesis, China University of Geosciences, Beijing, pp 77–96

Li Y, Lu XB, Wang YY, Zhang H, Cai ZX, Li DZ (2016) Hydrogeomorphologic characterization and evolution of the Early Hercynian karstification in Tahe Oilfield, the Tarim Basin (in Chinese with English abstract). Oil Gas Geol 37(5):674–683

Li Y, Lu XB, Cai ZX, Zhang H, Liu XF (2017) Development model of Hercynian cave system in karst canyon area of Tahe Oilfield, Tarim Basin (in Chinese with English abstract). J Palaeogeogr 19(2):364–372

Li YG (2007) Study on underground reservoir construction (in Chinese). China Environmental Science Press, Beijing, pp 1–27

Liu GR, Feng YD (2002) Research on water system of reservoir in karst area and its underground sub-system (in Chinese with English abstract). Int J Hydroelectric Energy 20(1):6–8

Liu Z, Li Q, Sun H, Wang J (2007) Seasonal, diurnal and storm-scale hydrochemical variations of typical epikarst springs in subtropical karst areas of SW China: soil $CO_2$ and dilution effects. J Hydrol 337(1–2):207–223. https://doi.org/10.1016/j.jhydrol.2007.01.034

Lu ZQ (2001) Research of karst and engineering geology in a karst area (in Chinese), chap 8. In: Engineering geology. China Water Resources and Hydropower Press, Beijing, pp 233–264

Ma RY, Liang H (2018) Application of Muskingum method in flood routing of Youjiang River based on interval inflow forecast (in Chinese with English abstract). Yangtze River 49(3):23–26. https://doi.org/10.16232/jcnki.1001-4179.2018.03.004

Ma X, Chen BY, Liu SH (2005) Treatment of special conditions of high-pressure grouting construction in karstified dam site area of Wujiangdu Hydropower Station (in Chinese with English abstract). Explor Eng (Rock Soil Drill Tunnel) 1:13–17

Meng D (2013) Qianzhong Water Project study of water transfer and economic accounting (in Chinese with English abstract). MSc Thesis, School of Architectural Engineering, Tianjin University, Tianjin, China, pp 13–21

Ministry of Water Resources (2012) Bulletin of first national census for water. Ministry of Water Resources, P.R. China, 20 pp

Nourani V (2017) An emotional ANN (EANN) approach to modeling rainfall-runoff process. J Hydrol 544:267–277. https://doi.org/10.1016/j.jhydrol.2016.11.033

Nourani V, Monadjemi P, Singh V (2007) Liquid analog model for laboratory simulation of rainfall–runoff process. J Hydrol Eng 12(3):246–255

Onder H, Yilmaz M (2005) Underground dams: a tool of sustainable development and management of groundwater resources. European Water 11(12):35–45

Ovchenikov AM (1958) Mineral water. Translated from Russian by Geological Publishing House, Beijing, China

Qian SF (2010) Present situation and protection analysis of karst underground reservoir (in Chinese). China New Technologies and Products 11: 109–110

Scudder T (2019) Large dams: long term impacts on riverine communities and free flowing rivers. Springer, Singapore

Press SM (2018) The atlas of China (in Chinese). SinoMaps Press, Beijing, pp 92–95

Song HZ, Qi FD (1992) Karst development characteristics and seepage control scheme design in Wujiangdu Dam site area (in Chinese with English abstract). J Hohai Univ 20(2):59–65

Stevanovic Z (2019) Karst waters in potable water supply: a global scale overview. Environ Earth Sci 78(662). https://doi.org/10.1007/s12665-019-8670-9

Tian H, Li SH, Jin ZS (1979) Report of the hydrogeological survey in Anshun District (in Chinese). Hydrogeological Investigation Report, The Geological Bureau of Guizhou Province, Guiyang, China, pp 28–46

Wada Y, Beek LPH, Kempen CM, Reckman JWTM, Vasak S, Bierkens MFP (2010) Global depletion of groundwater resources. Geophys Res Lett 37:L20402. https://doi.org/10.1029/2010GL044571

Wang SJ, Zhang XB, Bai XY (2015) An outline of karst geomorphology zoning in the karst areas of southern China (in Chinese with English abstract). Mountain Res 33(6):641–648. https://doi.org/10.16089/j.cnki.1008-2786.000079

Wang WF (1999) Study on the construction conditions of Maguan underground reservoir and its benefit at Puding, Guizhou (in Chinese with English abstract). Carsolog Sin 18(1):48–55

Wang X, Wang H, Wang WH (2000) Principle and application of artificial neural network (in Chinese). Northeast University Press, Shenyang, China, pp 51–68

Wei J, Yang LZ (1997) Study on the hydrogeological characteristics and comprehensive development and utilization of subterranean river systems in typical peak-cluster karst areas (in Chinese with English abstract). Geotech Invest Surveying 3:37–41

Wu TJ (2014) Research on the contribution of lateral inflow to floods in Three Gorges Reservoir (in Chinese with English abstract). MSc Thesis, Tsinghua University, Beijing, 95 pp

Yang LJ (2015) Study on multi-objective optimization operation of reservoir group based on periodically sequential decision (in Chinese with English abstract). MSc Thesis, China Institute of Water Resources and Hydropower Research, Beijing, China, pp 29–34

Ye SZ (1992) Calculation methods of hydrology and water conservancy (in Chinese). China Water and Power Press, Beijing, pp 256–280

Yuan DX, Zhu DH, Weng JT, Zhu XW, Han XR, Wang XY, Cai GH, Zhu YF, Cui GZ, Deng ZQ (1994) China karstology (in Chinese). Geological Publishing House, Beijing, 207 pp

Yuan Y (2015) Research on Optimal Water Resources Allocation and Water Rights Distribution in Central Guizhou Province (in Chinese with English abstract). MSc Thesis, Donghua University, Shanghai, China, pp 9–12

Zeng C, Yang R, Yang MM, Hu JC, Wu GH, Fan YH (2013) Artificial neural network simulation to zero flow of the Heilongtan Spring groups in Lijiang, China (in Chinese with English abstract). Carsolog Sin 32(4):391–397

Zeng C, Li ZJ, Wang Y, Li HY (2020) Early paleozoic tropical paleokarst geomorphology predating terrestrial plant growth in the Tahe Oilfield, Northwest China. Mar Pet Geol 122:1–16. https://doi.org/10.1016/j.marpetgeo.2020.104653

Zhang ZG (2006) Origin of karst, theoretical works on karst (in Chinese). Guangxi Normal University Press, Guilin, China, 285 pp

Zolotov AY, Ivanov V, Amelin V (2002) Methods and tools for analysis of liquid samples, chap 3. Comprehen Analyt Chem 36: 69–117. https://doi.org/10.1016/S0166-526X(02)80023-X